Using the inclinations of *Kepler* systems to prioritize new Titius–Bode-based exoplanet predictions

T. Bovaird,[1,2]⋆ C. H. Lineweaver[1,2,3] and S. K. Jacobsen[4]

[1]*Research School of Astronomy and Astrophysics, Australian National University, Canberra, ACT 2611, Australia*
[2]*Planetary Science Institute, Australian National University, Canberra, ACT, 2601, Australia*
[3]*Research School of Earth Sciences, Australian National University, Canberra, ACT, 2601, Australia*
[4]*Niels Bohr Institute, University of Copenhagen, Copenhagen, 1017, Denmark*

ABSTRACT

We analyse a sample of multiple-exoplanet systems which contain at least three transiting planets detected by the *Kepler* mission ('*Kepler* multiples'). We use a *generalized* Titius–Bode relation to predict the periods of 228 additional planets in 151 of these *Kepler* multiples. These Titius–Bode-based predictions suggest that there are, on average, 2 ± 1 planets in the habitable zone of each star. We estimate the inclination of the invariable plane for each system and prioritize our planet predictions by their geometric probability to transit. We highlight a short list of 77 predicted planets in 40 systems with a high geometric probability to transit, resulting in an expected detection rate of ∼15 per cent, ∼3 times higher than the detection rate of our previous Titius–Bode-based predictions.

Key words: planets and satellites: detection – planets and satellites: formation – planets and satellites: terrestrial planets – planet-disc interactions.

1 INTRODUCTION

The Titius–Bode (TB) relation's successful prediction of the period of Uranus was the main motivation that led to the search for another planet between Mars and Jupiter, e.g. Jaki (1972). This search led to the discovery of the asteroid Ceres and the rest of the asteroid belt. The TB relation may also provide useful hints about the periods of as-yet-undetected planets around other stars. In Bovaird & Lineweaver (2013, hereafter BL13), we used a *generalized* TB relation to analyse 68 multiplanet systems with four or more detected exoplanets. We predicted the existence of 141 new exoplanets in these 68 systems. Huang & Bakos (2014, hereafter HB14) performed an extensive search in the *Kepler* data for 97 of our predicted planets in 56 systems. This resulted in the confirmation of five of our predictions (Fig. 4 and Table 1).

In this paper, we perform an improved TB analysis on a larger sample of *Kepler* multiple-planet systems[1] to make new exoplanet orbital period predictions. We use the expected coplanarity of multiple-planet systems to estimate the most likely inclination of the invariable plane of each system. We then prioritize our original and new TB-based predictions according to their geometric probability of transiting. Comparison of our original predictions with the HB14 confirmations shows that restricting our predictions to

those with a high geometric probability to transit should increase the detection rate by a factor of ∼3 (Fig. 8).

As in BL13, our sample includes all *Kepler* multiplanet systems with four or more exoplanets, but to these we add three-planet systems if the orbital periods of the system's planets adhere better to the TB relation than the Solar system (equation 4 of BL13). Using these criteria we add 77 three-planet systems to the 74 systems with four or more planets. We have excluded three systems: KOI-284, KOI-2248 and KOI-3444 because of concerns about false positives due to adjacent-planet period ratios close to 1 and close binary hosts (Lissauer et al. 2011; Fabrycky et al. 2014; Lillo-Box, Barrado & Bouy 2014). We have also excluded the three-planet system KOI-593, since the period of KOI-593.03 was recently revised, excluding the system from our three-planet sample. Thus, we analyse 151 *Kepler* multiples, with each system containing 3, 4, 5 or 6 planets.

1.1 Coplanarity of exoplanet systems

Planets in the Solar system and in exoplanetary systems are believed to form from protoplanetary discs (e.g. Winn & Fabrycky 2014). The inclinations of the eight planets of our Solar system to the invariable plane are (in order from Mercury to Neptune) 6°3, 2°2, 1°6, 1°7, 0°3, 0°9, 1°0, 0°7 (Souami & Souchay 2012). Jupiter and Saturn contribute ∼86 per cent of the total planetary angular momentum and thus the angles between their orbital planes and the invariable plane are small: 0°3 and 0°9, respectively.

In a given multiple-planet system, the distribution of mutual inclinations between the orbital planes of planets is well described by

---

⋆ E-mail: timothy.bovaird@anu.edu.au
[1] Accessed on 2014 November 4: http://exoplanetarchive.ipac.caltech.edu/cgi-bin/TblView/nph-tblView?app=ExoTbls&config=cumulative.

Table 1. Systems with candidate detections by HB14 (in bold) plus KOI-1151 (Petigura, Howard & Marcy 2013a) and KOI-1860,[b] after planet predictions were made by BL13.

System	Predicted period (d)	Detected period (d)	Predicted radius ($R_\oplus$)	Detected radius ($R_\oplus$)
KOI-719	14 ± 2	15.77	≤ 0.7	0.42
KOI-1336	26 ± 3	27.51	≤ 2.4	1.04
KOI-1952	13 ± 2	13.27	≤ 1.5	0.85
KOI-2722[a]	16.8 ± 1.0	16.53	≤ 1.6	1.16
KOI-2859	5.2 ± 0.3	5.43	≤ 0.8	0.76
KOI-733	N/A	15.11	N/A	3.0
KOI-1151[a]	9.6 ± 0.7	10.43	≤ 0.8	0.7
KOI-1860[b]	25 ± 3	24.84	≤ 2.7	1.46

Notes. [a]Predicted by preprint of BL13 (draft uploaded 2013 Apr 11: http://arxiv.org/pdf/1304.3341v1.pdf), detected planet reported by *Kepler* archive and included in analysis of BL13.
[b]2014 October *Kepler* Archive update, during the drafting of this paper.

a Rayleigh distribution (Lissauer et al. 2011; Fang & Margot 2012; Figueira et al. 2012; Ballard & Johnson 2014; Fabrycky et al. 2014). For the ensemble of *Kepler* multiplanet systems, the mode of the Rayleigh distribution of *mutual inclinations* ($\phi_j - \phi_i$) is typically $\sim 1°$–$3°$ (Appendix A1 and Table A1). Thus, *Kepler* multiple-planet systems are highly coplanar. The Solar system is similarly coplanar. For example, the mode of the best-fitting Rayleigh distribution of the planet inclinations (ϕ_j) *relative to the invariable plane* in the Solar system is $\sim 1°$ (see Figs 1 and 2).[2]

The angle $\Delta\theta_j$ is a Gaussian distributed variable with a mean of 0 (centred around $\langle\theta\rangle$) and standard deviation $\sigma_{\Delta\theta}$. Based on previous analyses (Table A1), we assume the typical value $\sigma_{\Delta\theta} = 1°.5$. We use this angle to determine the probability of detecting additional transiting planets in each system.

Estimates of the inclination of a transiting planet come from the impact parameter b which is the projected distance between the centre of the planet at mid-transit and the centre of the star, in units of the star's radius,

$$b = \frac{a}{R_*} \cos i, \qquad (1)$$

where R_* is the radius of the star and a is the semimajor axis of the planet. For edge-on systems, typically $85° < i < 95°$. However, since we are unable to determine whether b is in the positive z direction or the negative z direction (Figs 1b and B1), we are unable to determine whether i is greater than or less than $90°$. By convention, for transiting planets the sign of b is taken as positive and thus the corresponding i values from equation (1) are taken as $i \leq 90°$.

The impact parameter is also a function of four transit light-curve observables (Seager & Mallén-Ornelas 2003); the period P, the transit depth ΔF, the total transit duration t_T, and the total transit duration minus the ingress and egress times t_F (the duration where the light curve is flat for a source uniform across its disc). Thus, the impact parameter can be written as

$$b = f(P, \Delta F, t_T, t_F). \qquad (2)$$

Eliminating b from equations (1) and (2) yields the inclination i as a function of observables,

$$i = \cos^{-1}\left[\frac{R_*}{a} f(P, \Delta F, t_T, t_F)\right]. \qquad (3)$$

From equation (1), we can see that for an impact parameter $b = 0$ (a transit through the centre of the star), we obtain $i = 90°$: an 'edge-on' transit.

The convention $i \leq 90°$ is unproblematic when only a single planet is found to transit a star but raises an issue when multiple exoplanets transit the same star, since the degree of coplanarity depends on whether the actual values of i_j ($j = 1, 2, \ldots, N$, where N is the number of planets in the system) are greater than or less than $90°$. For example, the actual values of i_j in a given system could be all $>90°$, all $<90°$ or some in-between combination. Although we do not know the signs of $\theta_j = 90° - i_j$ for individual planets, we can estimate the inclination of the invariable plane for each system, by calculating all possible permutations of the θ_j values for each system (see Appendix A2). In this estimation, we use the plausible assumption that the coplanarity of a system should not depend on the inclination of the invariable plane relative to the observer.

1.2 The probability of additional transiting exoplanets

We wish to develop a measure of the likelihood of additional transiting planets in our sample of *Kepler* multiplanet systems. The more edge-on a planetary system is to an observer on Earth, the greater the probability of a planet transiting at larger periods. Similarly, a larger stellar radius leads to a higher probability of additional transiting planets (although with a reduced detection efficiency). We quantify these tendencies under the assumption that *Kepler* multiples have a Gaussian opening angle $\sigma_{\Delta\theta} = 1°.5$ around the invariable plane, and we introduce the variable, $a_{\rm crit}$. Planets with a semimajor axis greater than $a_{\rm crit}$ have less than a 50 per cent geometric probability of transiting. More specifically, $a_{\rm crit}$ is defined as the semimajor axis where $P_{\rm trans}(a_{\rm crit}) = 0.5$ (equation B1) for a given system.

In a given system, a useful ratio for estimating the amount of semimajor axis space where additional transiting planets are more likely, is $a_{\rm crit}/a_{\rm out}$, where $a_{\rm out}$ is the semimajor axis of the detected planet in the system which is the furthest from the host star. The larger $a_{\rm crit}/a_{\rm out}$, the larger the semimajor axis range for additional transiting planets beyond the outermost detected planet. Values for this ratio less than 1 mean that the outermost detected planet is beyond the calculated $a_{\rm crit}$ value, and imply that additional transiting planets beyond the outermost detected planet are less likely. Fig. 3 shows the $a_{\rm crit}/a_{\rm out}$ distribution for all systems in our sample. The fact that this distribution is roughly symmetric around $a_{\rm crit}/a_{\rm out} \sim 1$ strongly suggests that the outermost *transiting* planets in *Kepler* systems are due to the inclination of the system to the observer, and are not really the outermost planets.

In Section 2, we discuss the follow-up that has been done on our BL13 planet detections. In Section 3, we show that the ~ 5 per cent follow-up detection rate of HB14 is consistent with selection effects and the existence of the predicted planets. In Section 4, we extend and upgrade the TB relation developed in BL13 and predict the periods of undetected planets in our updated sample. We then prioritize these predictions based on their geometric probability to transit and emphasize for further follow-up a subset of predictions with high transit probabilities. We also use TB predictions to estimate the average number of planets in the circumstellar habitable zone (HZ). In Section 5, we discuss how our predicted planet insertions affect the period ratios of adjacent planets and explore how period ratios are

[2] See Appendix A for an explanation of why the distribution of mutual inclinations is on average a factor of $\sqrt{2}$ wider than the distribution of the angles ϕ_j in Fig. 1, between the invariable plane of the system and the orbital planes of the planets.
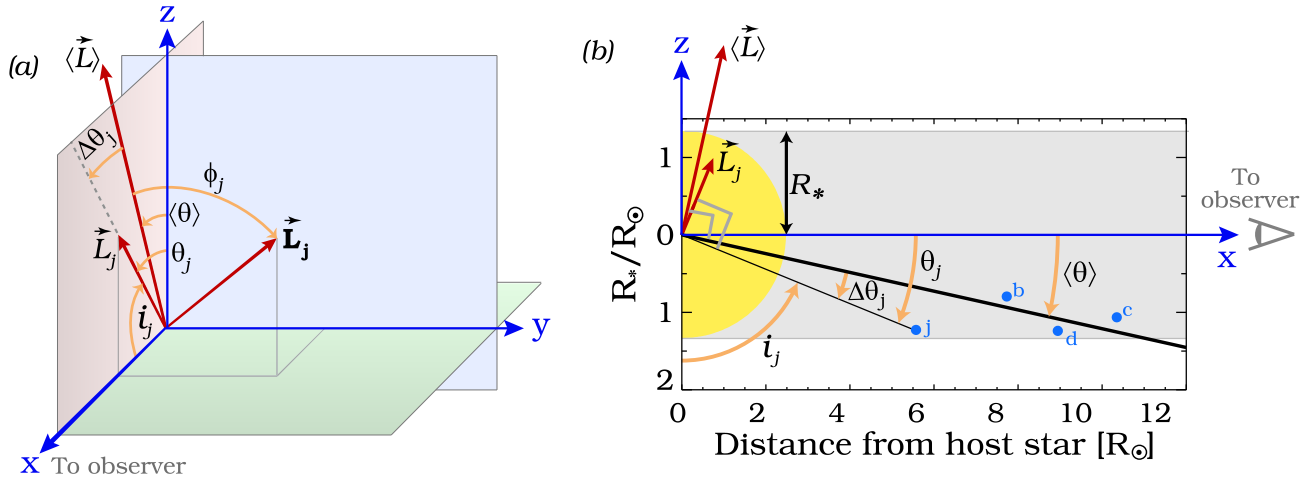
Figure 1. Panel (a): our coordinate system for transiting exoplanets. The *x*-axis points towards the observer. L_j is the 3D angular momentum of the *j*th planet, and is perpendicular to the orbital plane of the *j*th planet. $\langle L \rangle$ is the sum of the angular momenta of all detected planets (equation A2) and is perpendicular to the invariable plane of the system. We have chosen the coordinate system without loss of generality such that $\langle L \rangle$ has no component in the *y* direction. ϕ_j is the angle between L_j and $\langle L \rangle$. Let $\tilde{L}_j$ be the projection of L_j on to the *x*–*z* plane. $\Delta\theta_j$ is the angle between $\langle L \rangle$ and $\tilde{L}_j$. $\langle \theta \rangle$ is the angle between the *z*-axis and $\langle L \rangle$. i_j is the inclination of the planet (equation 3). $\theta_j = 90 - i_j$ and is the angle between the *z*-axis and $\tilde{L}_j$ such that $\theta_j = \langle\theta\rangle + \Delta\theta_j$ (equation A4). Panel (b) shows the *x*–*z* plane of panel (a) with the *y*-axis pointing into the paper. The observer is to the right. The grey shaded region represents the 'transit region' where the centre of a planet will transit its host star as seen by the observer (impact parameter $b \leq 1$, see equation 1). Four planets, b, c, d and j, are represented by blue dots. The intersection of the orbital plane of the *j*th planet with the *x*–*z* plane is shown (thin black line). All angles shown in panel (a) (with the exception of ϕ_j) are also shown in panel (b). The thick line is the intersection of the invariable plane of the system with the *x*–*z* plane. Because we are only dealing with systems with multiple transiting planets, all these angles are typically less than a few degrees but are exaggerated here for clarity.
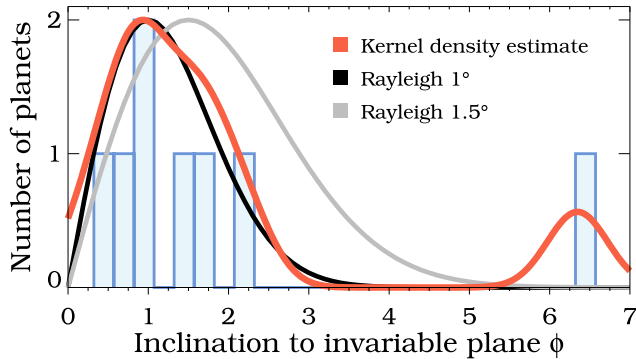

Figure 2. The coplanarity of planets in the Solar system relative to the invariable plane. With the exception of Mercury, the angles between the orbital planes of the planets and the invariable plane are well represented by a Rayleigh distribution with a mode of $\sim 1°$.

tightly dispersed around the mean period ratio within each system. In Section 6, we summarize our results.

2 FOLLOW-UP OF BL13 PREDICTIONS

BL13 used the approximately even logarithmic spacing of exoplanet systems to make predictions for the periods of 117 additional candidate planets in 60 *Kepler* detected systems, and 24 additional predictions in 8 systems detected via radial velocity (7) and direct imaging (1), which we do not consider here. NASA Exoplanet Archive data updates, confirmed our prediction of KOI-2722.05 (Table 1).

HB14 used the planet predictions made in BL13 to search for 97 planets in the light curves of 56 *Kepler* systems. Within these 56 systems, BL13 predicted the period and maximum radius: the largest radius which would have evaded detection, based on the lowest signal-to-noise of the detected planets in the same system.
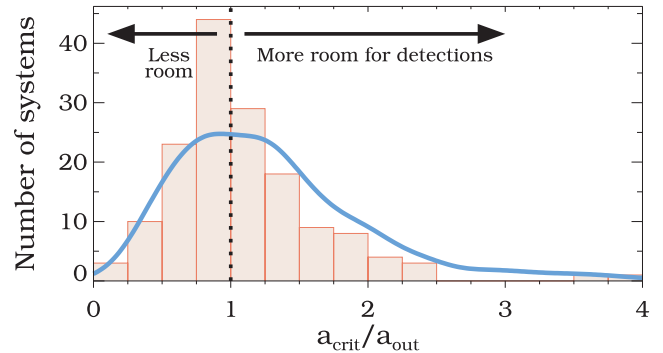

Figure 3. Histogram of the a_{crit}/a_{out} values for our sample of *Kepler* multiples. The distribution peaks for a ratio just below 1. Approximately half of the systems lie to the right of 1. For these systems, if there are planets with semimajor axes *a* such that $a_{out} < a < a_{crit}$, then the geometric probability of them transiting is greater than 50 per cent. Note that this does not account for the detectability of these planets (e.g. they could be too small to detect). The majority of the predicted planets that are insertions ($a < a_{out}$) have geometric transit probabilities greater than 50 per cent, when $a_{crit}/a_{out} < 1$. Systems on the right have more room for detections, and in general, predicted planets in these systems have higher values of P_{trans}. The blue curve is the expected distribution of our sample of *Kepler* multiples if they all have planets at TB-predicted semimajor axes extrapolated out to $\sim 4 \times a_{crit}$. The blue curve is consistent with the observed distribution, indicating that our a_{crit}/a_{out} distribution is consistent with the system in our sample containing more planets than have been detected.

Predicted planets were searched for using the *Kepler* Quarter 1 to Quarter 15 long-cadence light curves, giving a baseline exceeding 1000 d. Once the transits of the already known planets were detected and removed, transit signals were visually inspected around the predicted periods.

Of the 97 predicted planets searched for by HB14, 5 candidates were detected within $\sim 1\sigma$ of the predicted periods (5 planets of the
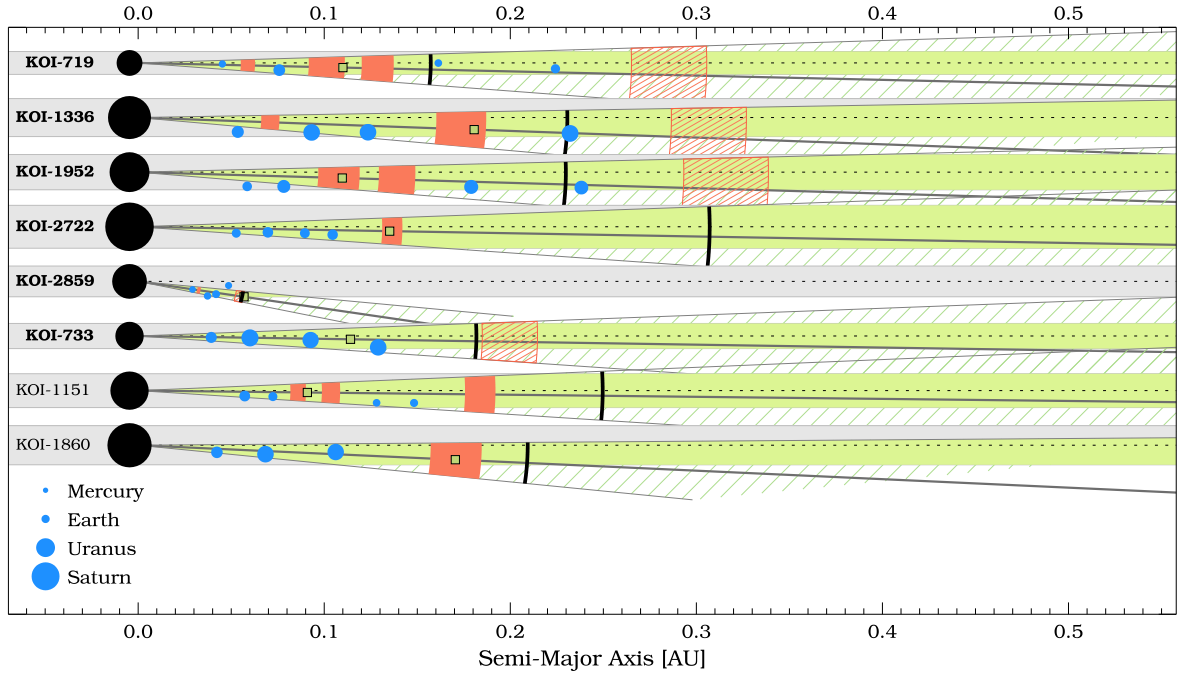
Figure 4. Exoplanet systems where an additional candidate was detected after a TB relation prediction was made (see Table 1). The systems are shown in descending order of a_{crit}/a_{out}. Previously known planets are shown as blue circles. The predictions of BL13 and their uncertainties are shown by the red filled rectangles if the P_{trans} value of the predicted planet is ≥ 0.55 (equation B1 and Fig. 8), or by red hatched rectangles otherwise. The new candidate planets are shown as green squares. The critical semimajor axis a_{crit} (Section 1.2), beyond which $P_{trans}(a_{crit}) < 0.5$, is shown by a solid black arc.
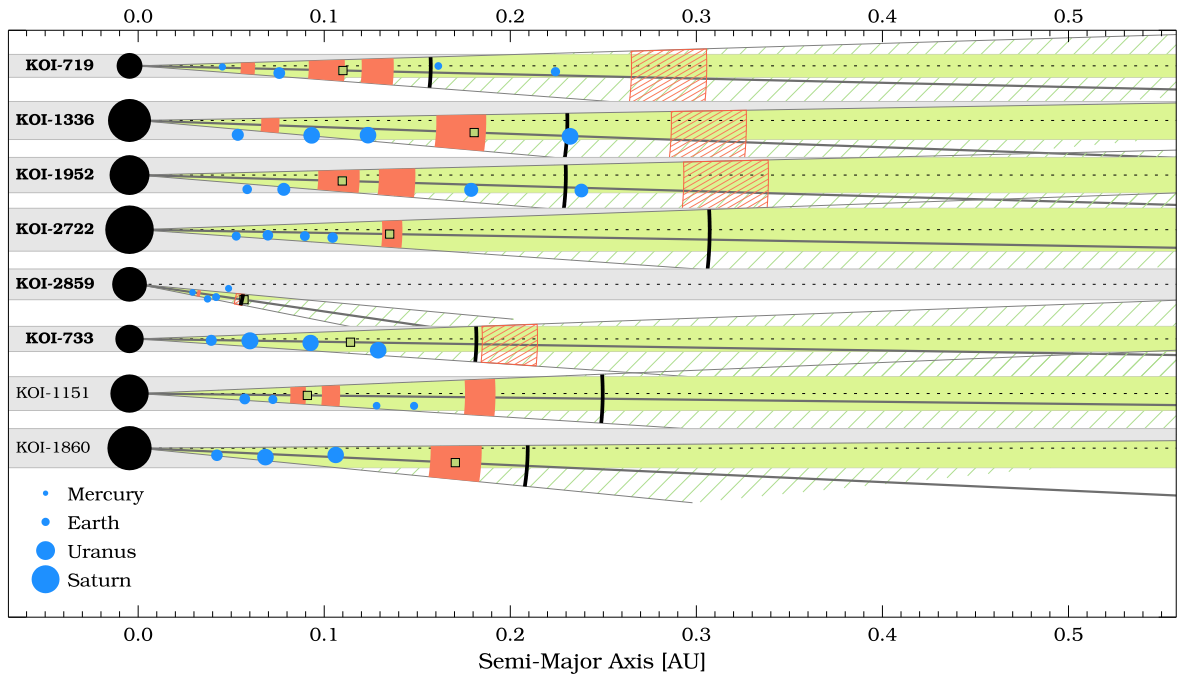
Figure 5. Same as Fig. 4 except here our TB predictions are based on γ with n_{ins}^2 (equation 9) rather than on the γ with n_{ins} of equation 5 of BL13. Comparing Fig. 4 with this figure, in the KOI-719 system the number of predicted planets goes from 4 to 2, while in KOI-1151 the number of predicted planets goes from 3 to 2. In both cases the detected planet is more centrally located in the predicted region. The uncertainties (width of red rectangles) in Fig. 4 and Table 1, are slightly wider than Fig. 5 due to excessive rounding of predicted period uncertainties for some systems in BL13.

6 planets in bold in Table 1, see also Fig. 4). Notably all new planet candidates have Earth-like or lower planetary radii. One additional candidate was detected in KOI-733 which is incompatible with the predictions of BL13. This candidate is unique in that it should

have been detected previously, based on the signal to noise of the other detected planets in KOI-733. In Table 1, the detected radii are less than the maximum predicted radii in each case. The new candidate in KOI-733 has a period of 15.11 d and a radius of
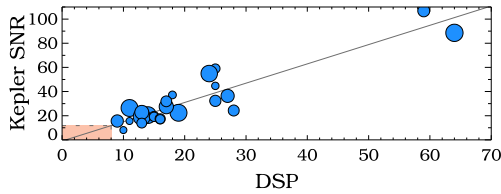
Figure 6. Reported dip significance parameter (DSP) from Table 1 of HB14 for previously known exoplanets in the five systems with a new detection. A linear trend can be seen for the DSP and the SNR as reported by the Kepler team (Christiansen et al. 2012). HB14 required planet candidates to have a DSP > 8 to survive their vetting process. The sizes of the blue dots correspond to the same planetary radii representation used to make Figs 11–14.

3 $R_{\oplus}$. At this period, the maximum radius to evade detection should have been 2.2 $R_{\oplus}$. With the possible exception of KOI-1336 where a dip significance parameter (DSP; Kovács & Bakos 2005) was not reported, all detected candidates have a DSP of $\geq$ 8, which roughly corresponds to a *Kepler* signal-to-noise ratio (SNR; Christiansen et al. 2012) of $\gtrsim$ 12 (see Fig. 6). HB14 required DSP > 8 for candidate transit signals to survive their vetting process.

3 IS A 5 PER CENT DETECTION RATE CONSISTENT WITH SELECTION EFFECTS?

From a sample of 97 BL13 predictions, HB14 confirmed 5. However, based on this ∼5 per cent detection rate, HB14 concluded that the predictive power of the TB relation used in BL13 was questionable. Given the selection effects, how high a detection rate should one expect? We do not expect all planet predictions to be detected. The predicted planets may have too large an inclination to transit relative to the observer. Additionally, there is a completeness factor due to the intrinsic noise of the stars, the size of the planets and the techniques for detection. This completeness for *Kepler* data has been estimated for the automated light-curve analysis pipeline TERRA (Petigura et al. 2013a). Fig. 7 displays the TERRA pipeline injection/recovery completeness. After correcting for the radius and noise of each star, relative to the TERRA sample in Fig. 7, the planet detections in Table 1 have an average detection completeness in the TERRA pipeline of ∼24 per cent. That is, if all of our predictions were correct and if all the planets were in approximately the same region of period and radius space as the green squares in Fig. 7, and if all of the planets transited, we would expect a detection rate of ∼24 per cent using the TERRA pipeline. It is unclear how this translates into a detection rate for a manual investigation of the light curves motivated by TB predictions.

We wish to determine, from coplanarity and detectability arguments, how many of our BL13 predictions we would have expected to be detected. An absolute number of expected detections is most limited by the poorly known planetary radius distribution below 1 $R_{\oplus}$ (Howard et al. 2012; Dong & Zhu 2013; Dressing & Charbonneau 2013; Fressin et al. 2013; Petigura, Marcy & Howard 2013b; Foreman-Mackey, Hogg & Morton 2014; Morton & Swift 2014; Silburt, Gaidos & Wu 2015). Large uncertainties about the shape and amplitude of the planetary radius distribution of rocky planets with radii less than 1 $R_{\oplus}$ make the evaluation of TB-based exoplanet predictions difficult. Since the TB relation predicted the asteroid belt ($M_{asteroid} < 10^{-3} M_{Earth}$) there seems to be no lower mass limit to the objects that the TB relation can predict. This makes estimation of the detection efficiencies strongly dependent on assumptions about the frequency of planets at small radii.
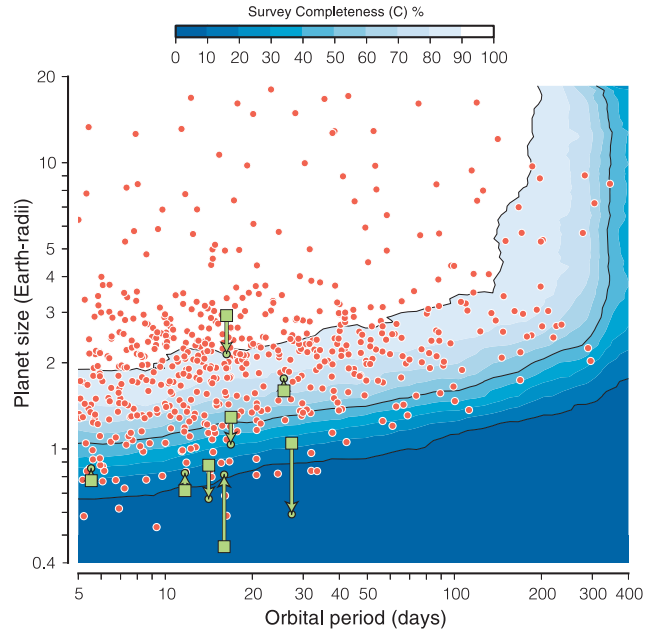
Figure 7. The simulated detection completeness of the new candidate planets in the TERRA pipeline (modified from fig. 1 of Petigura et al. 2013a). Here, we overplot as green squares, the eight planets listed in Table 1. The completeness curves are averaged over all stellar noise and stellar radii in the Petigura et al. (2013a) sample (the 42 000 least noisy *Kepler* stars). Green circles indicate the 'effective radius' of the new candidates, based on the noise and radius of their host star in comparison to the median of the quietest 42 000 sample. From the signal to noise, the effective radius can be calculated by $R_{p, \, \text{eff}}/R_p = (R_*/R_{\star, \, \text{median}}) \times (\text{CDPP}/\text{CDPP}_{\text{median}})^{1/2}$, where CDPP is the combined differential photometric precision defined in Christiansen et al. (2012). Taking a subset of 42 000 stars from the *Kepler* input catalogue with the lowest 3-h CDPP (approximately representative of the sample in the figure), we obtain $\text{CDPP}_{\text{median}} \approx 60 \, \text{ppm}$ and $R_{\star, \, \text{median}} \approx 1.15 \, R_{\odot}$. Using the effective radius and excluding the outlier KOI-733, the mean detection completeness for the seven candidate planets in Table 1 is ∼24 per cent.

Let the probability of detecting a planet, P_{detect}, be the product of the geometric probability to transit P_{trans} as seen by the observer (Appendix B) and the probability P_{SNR} that the planetary radius is large enough to produce an SNR above the detection threshold,

$$P_{\text{detect}} = P_{\text{trans}} \; P_{\text{SNR}}. \tag{4}$$

The geometric probability to transit, P_{trans}, is defined in equation (B1) and illustrated in Figs 1 and B1. The five confirmations from our previous TB predictions are found in systems with a much higher than random probability of transit (Fig. 8). This is expected if our estimates of the invariable plane are reasonable.

To estimate P_{SNR}, we first estimate the probability that the radius of the planet will be large enough to detect. In BL13 we estimated the maximum planetary radius, R_{max}, for a hypothetical undetected planet at a given period, based on the lowest signal-to-noise of the detected planets in the same system. We now wish to estimate a minimum radius that would be detectable, given the individual noise of each star. We refer to this parameter as R_{min}, which is the minimum planetary radius that *Kepler* could detect around a given star (using a specific SNR threshold). For each star we used the mean CDPP (combined differential photometric precision) noise from Q1–Q16. When the number of transits is not reported, we use the approximation $N_{\text{trans}} \approx T_{\text{obs}} f_0/P$, where T_{obs} is the total observing time and f_0 is the fractional observing uptime, estimated at ∼0.92 for the *Kepler* mission (Christiansen et al. 2012).
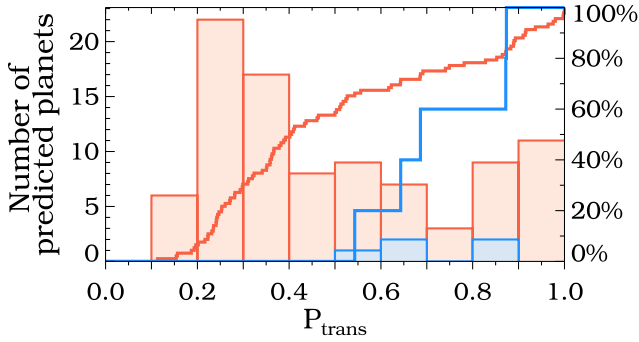
Figure 8. Histogram of P_{trans} (equation B1), the geometric probability of transit, for the 97 predicted planets from BL13, that were followed up by HB14. The blue histogram represents the five new planets detected by HB14 (Table 1). As expected, the detected planets have high P_{trans} values compared to the entire sample. The red and blue solid lines represent the empirical cumulative distribution function for the two distributions. A K–S test of the two distributions yields a p-value of 1.8×10^{-2}. Thus, P_{trans} can be used to prioritize our predictions and increase their probability of detection.

The probability P_{SNR} depends on the underlying planetary radius probability density function. We assume a density function of the form:

$$f(R) = \frac{df}{d\log R} = \begin{cases} k(\log R)^\alpha, & R \geq 2.8 \, R_\oplus \\ k(\log 2.8)^\alpha, & R < 2.8 \, R_\oplus \end{cases}, \quad (5)$$

where $k = 2.9$ and $\alpha = -1.92$ (Howard et al. 2012). The discontinuous distribution accounts for the approximately flat number of planets per star in logarithmic planetary radius bins for $R \lesssim 2.8 \, R_\oplus$ (Dong & Zhu 2013; Fressin et al. 2013; Petigura et al. 2013b; Silburt et al. 2015). For $R \lesssim 1.0 \, R_\oplus$ the distribution is poorly constrained. For this paper, we extend the flat distribution in log R down to a minimum radius $R_{low} = 0.3 \, R_\oplus$. It is important to note that for the Solar system, the poorly constrained part of the planetary radius distribution contains 50 per cent of the planet population. For reference the radius of Ceres, a 'planet' predicted by the TB relation applied to our Solar system has a radius $R_{Ceres} = 476 \, \text{km} = 0.07 R_\oplus$.

The probability that the hypothetical planet has a radius that exceeds the SNR detection threshold is then given by

$$P_{SNR} = \frac{\int_{R_{min}}^{R_{max}} f(R) \, dR}{\int_{R_{low}}^{R_{max}} f(R) \, dR}. \quad (6)$$

We do not integrate beyond R_{max} since we expect a planet with a radius greater than R_{max} would have already been detected. We define R_{max} by

$$R_{max} = R_{minSNR} \left(\frac{P_{predict}}{P_{minSNR}} \right)^{1/4}, \quad (7)$$

where R_{minSNR} and P_{minSNR} are the radius and period respectively of the detected planet with the lowest signal-to-noise in the system. $P_{predict}$ is the period of the predicted planet. R_{min} depends on the SNR in the following way:

$$R_{min} = R_* \sqrt{SNR_{th} \, CDPP} \left(\frac{3 \, h}{n_{tr} \, t_T} \right)^{1/4}, \quad (8)$$

where SNR_{th} is the SNR threshold for a planet detection, n_{tr} is the number of expected transits at the given period and t_T is the transit duration in hours. See Fig. 9 for an illustration of how the integrals in P_{SNR} (equation 6) depend on the planet radii limits, R_{min} and R_{low}.

While P_{trans} is well defined, P_{SNR} is dependent on the SNR threshold chosen (SNR_{th}), the choice of R_{low} and the poorly constrained
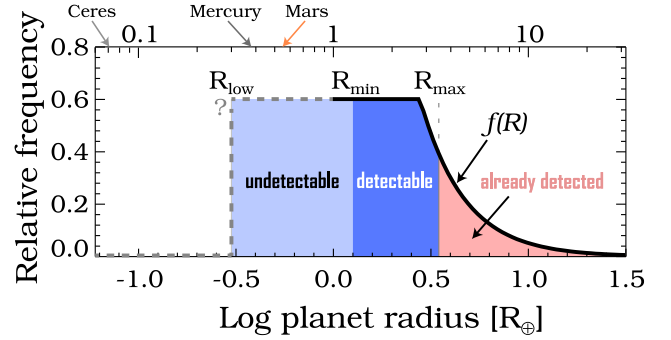
Figure 9. The assumed distribution of planetary radii described in Section 3. The distribution is poorly constrained below 1 $R_\oplus$, indicated by the grey dashed line. For low-mass stars, the planetary radius distribution may decline below 0.7 $R_\oplus$ (Dressing & Charbonneau 2013; Morton & Swift 2014). Alternative estimations show the planetary radius distribution continuing to increase with smaller radii (continuing the flat logarithmic distribution), down to 0.5 $R_\oplus$ (Foreman-Mackey et al. 2014). For our analysis we have extrapolated the flat distribution (in log R) down to R_{low}. We indicate three regions for a hypothetical system at a specific predicted period. The 'already detected' region refers to the range of planetary radii which should already have been detected, based on the lowest SNR of the detected planets in that system. R_{min} is the smallest radius which could produce a transit signal that exceeds the detection threshold, and is the boundary between the undetectable and detectable regions.
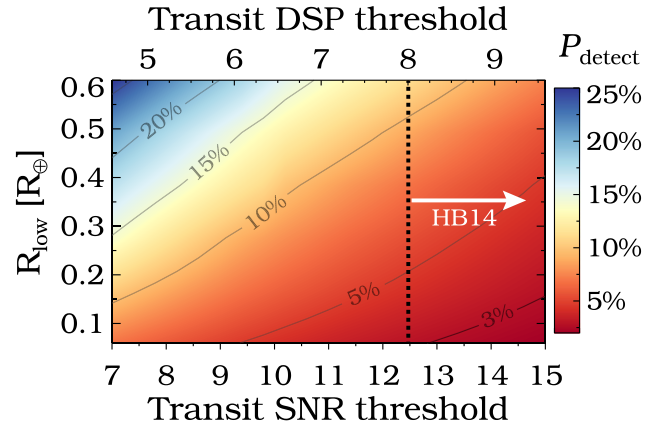
Figure 10. The mean detection rate P_{detect} (equation 4) of the BL13 predictions is dependent on the transit signal-to-noise threshold (SNR_{th} in equation 8) used in light-curve vetting (x-axis), and on the probability of low-radii planets, i.e. on how far the flat logarithmic planetary radius distribution in Fig. 9 should be extrapolated (R_{low} on the y-axis). For example, in the denominator of equation (6), integrating down to a radius R_{low} of 0.6 $R_\oplus$ and setting an SNR threshold of 7 (which sets R_{min} in the numerator) gives an expected detection fraction of $\sim$25 per cent (blue values in the upper left of the plot). Integrating down to a radius of 0.2 $R_\oplus$ and having a DSP threshold of 8 (converted from SNR according to Fig. 6) gives an expected detection fraction of $\sim$5 per cent (red values in the lower right).

shape of the planetary radius distribution below 1 $R_\oplus$. This is demonstrated in Fig. 10, where the mean P_{detect} from the predictions of BL13 (for DSP > 8) can vary from $\sim$2 to $\sim$11 per cent. Performing a K–S test on P_{SNR} values (analogous to that in Fig. 8) indicates that the P_{SNR} values for the subset of our BL13 predictions that were detected, are drawn from the same P_{SNR} distribution as all of the predicted planets. For this reason we use only P_{trans}, the geometric probability to transit, to prioritize our new TB relation predictions. We emphasize a subset of our predictions which have

a P_{trans} value ≥ 0.55, since all of the confirmed predictions of BL13 had a P_{trans} value above this threshold. Only $\sim 1/3$ of the entire sample have P_{trans} values this high. Thus, the ~ 5 per cent detection rate should increase by a factor of ~ 3 to ~ 15 per cent for our new high-P_{trans} subset of planet period predictions.

4 UPDATED PLANET PREDICTIONS

4.1 Method and inclination prioritization

We now make updated and new TB relation predictions in all 151 systems in our sample. If the detected planets in a system adhere to the TB relation better than the Solar system planets (χ^2/d.o.f. < 1.0, equation 4 of BL13), we only predict an extrapolated planet, beyond the outermost detected planet. If the detected planets adhere worse than the Solar system, we simulate the insertion of up to nine hypothetical planets into the system, covering all possible locations and combinations, and calculate a new χ^2/d.o.f. value for each possibility. We determine how many planets to insert, and where to insert them, based on the solution which improves the system's adherence to the TB relation, scaled by the number of inserted planets squared. This protects against overfitting (inserting too many planets, resulting in too good a fit). In equation 5 of BL13, we introduced a parameter γ, which is a measure of the fractional amount by which the χ^2/d.o.f. improves, divided by the number of planets inserted. Here, we improve the definition of γ by dividing by the square of the number of planets inserted,

$$\gamma = \frac{\left(\frac{\chi_i^2 - \chi_f^2}{\chi_f^2}\right)}{n_{ins}^2}, \qquad (9)$$

where χ_i^2 and χ_f^2 are the χ^2 of the TB relation fit before and after planets are inserted, respectively, while n_{ins} is the number of inserted planets.

Importantly, when we calculate our γ value by dividing by the number of inserted planets squared, rather than the number of planets, we still predict the BL13 predictions that have been detected. In two of these systems fewer planets are predicted and as a result the new predictions agree better with the location of the detected candidates. This can be seen by comparing Figs 4 and 5.

We compute P_{trans} for each planet prediction in our sample of 151 *Kepler* systems. We emphasize the 40 systems where at least one inserted planet in that system has $P_{trans} \geq 0.55$. Period predictions for this subset of 40 systems are displayed in Table C11 and Figs 11–13. As discussed in the previous section, we expect a detection rate of ~ 15 per cent for this high-P_{trans} sample. Predictions for all 228 planets (regardless of their P_{trans} value) are shown in Table C2 2 (where the systems are ordered by the maximum P_{trans} value in each system).

4.2 Average number of planets in circumstellar HZ

Since the search for earth-sized rocky planets in circumstellar HZ is of particular importance, in Fig. 14, for a subset of *Kepler* multiples whose predicted (extrapolated) planets extend to the HZ, we have converted the semimajor axes of detected and predicted planets into effective temperatures (as in fig. 6 of BL13). One can see in Fig. 14 that the HZ (shaded green) contains between 0 and 4 planets. Thus, if the TB relation is approximately correct, and if *Kepler* multiplanet systems are representative of planetary systems in general, there are on average ~ 2 HZ planets per star.

More specifically, in Table 2, we estimate the number of planets per star in various 'HZ', namely (1) the range of T_{eff} between Mars and Venus (assuming an albedo of 0.3), displayed in Fig. 14 as the green shaded region, (2) the Kopparapu et al. (2013) 'optimistic' and (3) 'conservative' HZ ('recent Venus' to 'early Mars', and 'runaway greenhouse' to 'maximum greenhouse', respectively). We find, on average, 2 ± 1 planets per star in the 'HZ', almost independently of which of the three HZs one is referring to. Using our estimates of the maximum radii for these predominantly undetected (but predicted) planets, as well as the planetary radius distribution of Fig. 9, we estimate that on average, $\sim 1/6$ of these ~ 2 planets, or ~ 0.3, are 'rocky'. We have assumed that planets with $R \leq 1.5\,R_{\oplus}$ are rocky (Rogers 2014; Wolfgang & Lopez 2014).

5 ADJACENT PLANET PERIOD RATIOS

HB14 concluded that the percentage of detected planets (~ 5 per cent) was on the lower side of their expected range (~ 5–20 per cent) and that the TB relation may overpredict planet pairs near the 3:2 mean-motion resonance (compared to systems which adhered to the TB relation better than the Solar system, without any planet insertions, i.e. χ^2/d.o.f ≤ 1). There is some evidence that a peak in the distribution of period ratios around the 3:2 resonance is to be expected from *Kepler* data, after correcting for incompleteness (Steffen & Hwang 2014). In this section, we investigate the period ratios of adjacent planets in our *Kepler* multiples before and after our new TB relation predictions are made.

We divide our sample of *Kepler* multiples into a number of subsets. Our first subset includes systems which adhere to the TB relation better than the Solar system (where we only predict an extrapolated planet beyond the outermost detected planet). Systems which adhere to the TB relation worse than the Solar system we divide into two subsets, before and after the planets predicted by the TB relation were inserted. Adjacent planet period ratios can be misleading if there is an undiscovered planet between two detected planets, which would reduce the period ratios if it was included in the data. To minimize this incompleteness, we also construct a subset of systems which are the most likely to be completely sampled (unlikely to contain any additional transiting planets within the range of the detected planet periods).

Systems which adhere to the TB relation better than the Solar system (χ^2/d.o.f ≤ 1) were considered by HB14 as being the sample of planetary systems that were most complete and therefore had a distribution of adjacent planet period ratios most representative of actual planetary systems. However, the choice of BL13 to normalize the TB relation to the Solar system's χ^2/d.o.f is somewhat arbitrary. The Solar system's χ^2/d.o.f is possibly too high to consider all those with smaller values of χ^2/d.o.f to be completely sampled.

We want to find a set of systems which are unlikely to host any additional planets between adjacent pairs, due to the system being dynamically full (Hayes & Tremaine 1998). We do this by identifying the systems where two or more sequential planet pairs are likely to be unstable when a massless test particle is inserted between each planet pair (dynamical spacing $\Delta < 10$; Gladman 1993; BL13).

The dynamical spacing Δ is an estimate of the stability of adjacent planets. If inserting a test particle between a detected planet pair results in either of the two new Δ values being less than 10, we consider the planet pair without the insertion to be complete. That is, there is unlikely to be room, between the detected planet pair, where an undetected planet could exist without making the planet pair dynamically unstable. Therefore, since the existence of
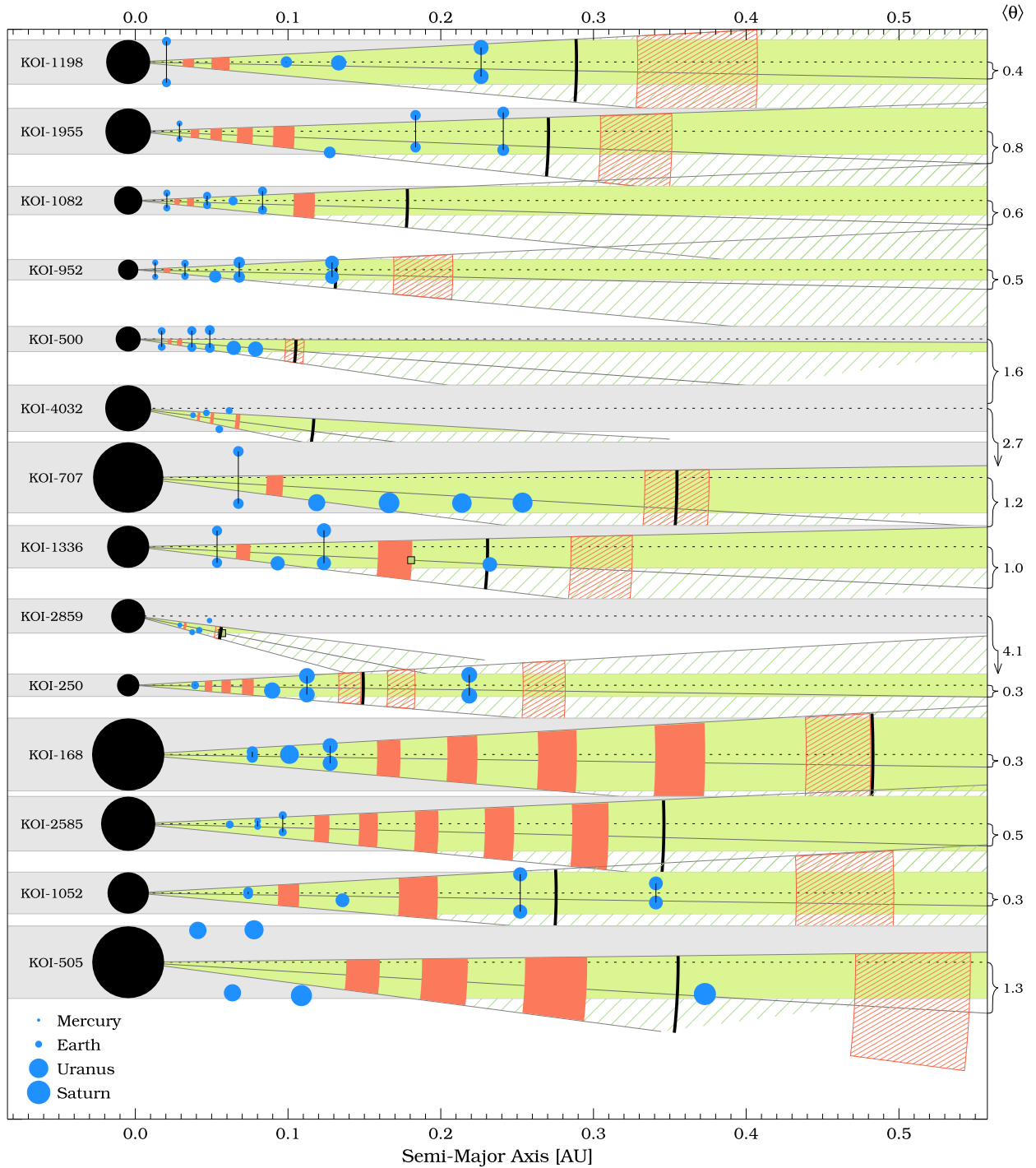
Figure 11. The architectures and invariable plane inclinations for *Kepler* systems in our sample which contain at least one planet with a geometric probability to transit $P_{\text{trans}} \geq 0.55$. There are 40 such systems out of the 151 in our sample. The 14 with the highest P_{trans} values are plotted here. The remaining 26 are plotted in the next two figures. The order of the systems (from top to bottom) is determined by the highest P_{trans} value in each system. The thin horizontal dotted line represents the line of sight to Earth, i.e. where the i value of a planet would be $90°$. The thick grey line in each system is our estimate of the invariant plane angle, $\langle\theta\rangle$ (Appendix A2). The value of $\langle\theta\rangle$ is given in degrees to the right of each panel (see also Fig. A1). The green wedge has an opening angle $\sigma_{\Delta\theta} = 1°5$ and is symmetric around the invariable plane, but is also limited to the grey region where a planet can be seen to transit from Earth ($b \leq 1$, equation 1). The thick black arc indicates the a_{crit} value beyond which less than 50 per cent of planets will transit (equation B1). Predicted planets and their uncertainties are shown by solid red rectangles if the P_{trans} value of the predicted planet is ≥ 0.55, or by red hatched rectangles otherwise. Thus, the 77 solid red rectangles in the 40 systems shown in Figs 11–13 make up our short list of highest priority predictions (Table C11). Our estimate of the most probable inclination ambiguities in a system are represented by vertically separated pairs of blue dots, connected by a thin black line (see Appendix A2).
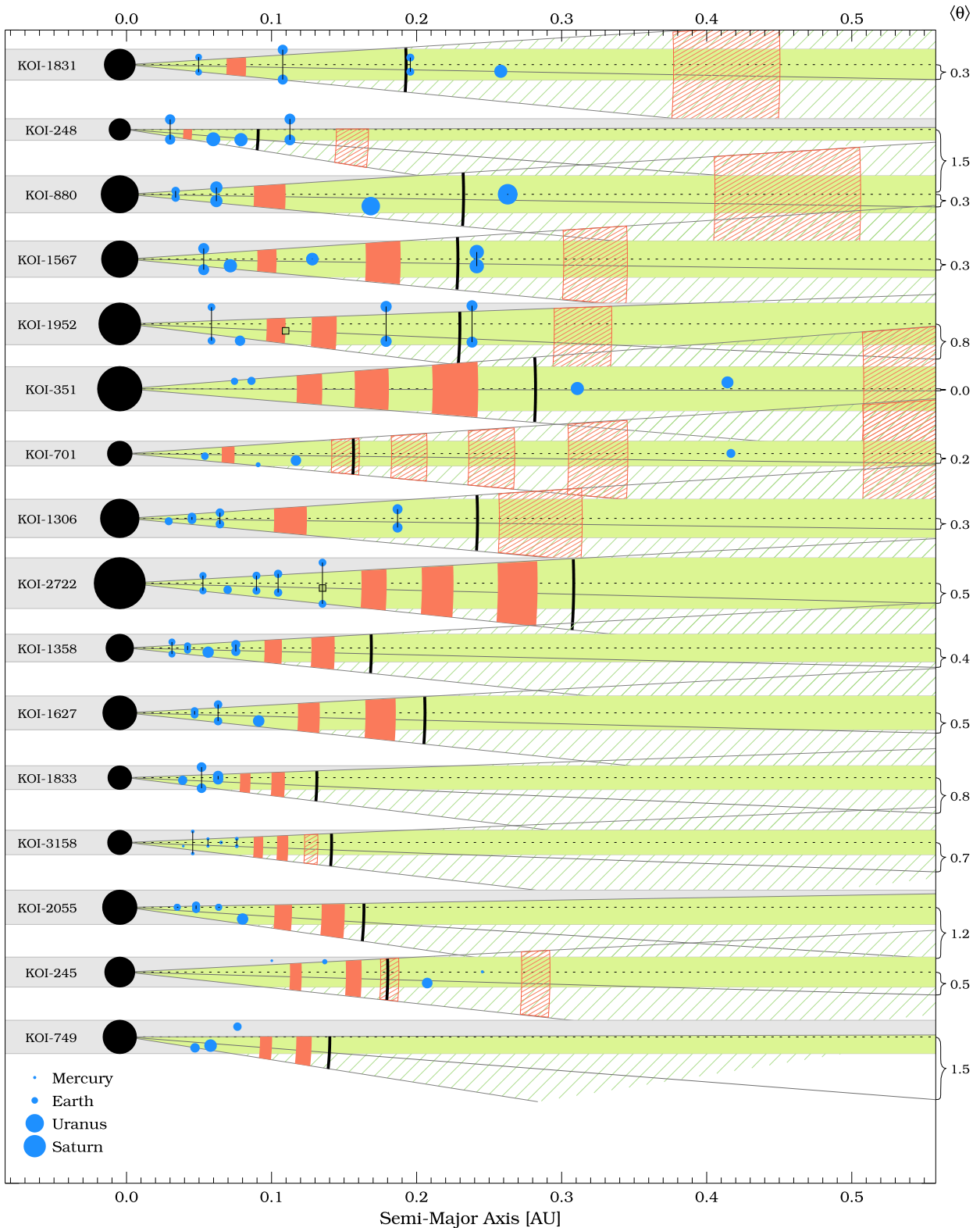
Figure 12. The same as Fig. 11 but for the next 16 systems in our sample which have at least one planet with $P_{trans} \geq 0.55$. Note that some of the new detected planets from the predictions of BL13 have been included in the *Kepler* data archive (see Table 1), and that these planets are included in our analysis.

an undetected planet between the planet pair is unlikely, we refer to the planet pair as 'completely sampled'. Estimating completeness based on whether a system is dynamically full is a reasonable approach, since there is some evidence that the majority of

systems are dynamically full (e.g. Barnes & Raymond 2004). For *Kepler* systems in particular, Fang & Margot (2013) concluded that *at least* 45 per cent of four-planet *Kepler* systems are dynamically packed.
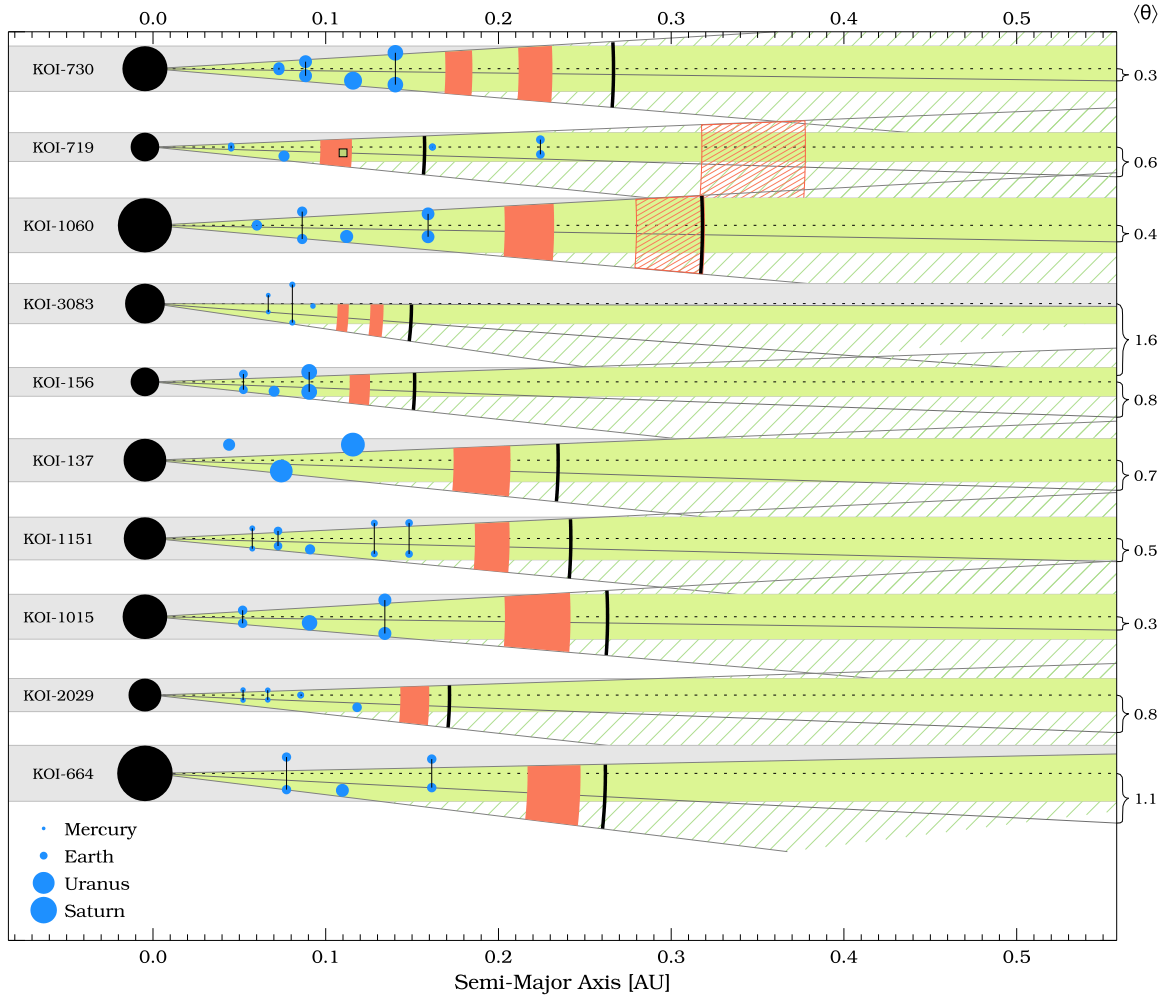
Figure 13. The same as Figs 11 and 12 but for the remaining 10 systems in our sample which have at least one planet with $P_{trans} \geq 0.55$.

If at least two sequential adjacent-planet pairs (at least three sequential planets) satisfy this criteria, we add the subset of the system which satisfies this criteria to our 'most complete' sample. We use this sample to analyse the period ratios of *Kepler* systems. The period ratios of the different samples described above are shown in Fig. 15.

One criticism from HB14 was that the TB relation from BL13 inserted too many planets. To address this criticism we have redefined γ to be divided by the number of inserted planets squared (denominator of equation 9). This introduces a heavier penalty for inserting planets. Fig. 15 displays the distributions of period ratios when using the γ from BL13 and the new γ of equation (9) (panels b and c, respectively). When using our newly defined γ, the mean χ^2/d.o.f. (displayed on the left-hand side of the panels), more closely resembles that of our 'most complete sample' (panel e).

Since each panel in Fig. 15 represents a mixture of planetary systems with different distributions of period ratios, Fig. 16 may be a better way to compare these different samples and their adherence to the TB relation. For each planetary system in each panel in Fig. 15, we compute the mean adjacent-planet period ratio. Fig. 16 shows the distribution of the offsets from the mean period ratio of each system. How peaked a distribution is, is a good measure of how well that distribution adheres to the TB relation. A delta function peak at an offset of zero, would be a perfect fit. The period ratios of adjacent-

planet pairs in our dynamically full 'most complete sample' (green in Fig. 16) display a significant tendency to cluster around the mean ratios. This clustering is the origin of the usefulness of the TB relation to predict the existence of undetected planets. The proximity of the thick blue curve to the green distribution is a measure of how well our TB predictions can correct for the incompleteness in *Kepler* multiple-planet systems and make predictions about the probable locations of the undetected planets.

6 CONCLUSION

HB14 investigated the TB relation planet predictions of Bovaird & Lineweaver (2013) and found a detection rate of ∼5 per cent (5 detections from 97 predictions). Apart from the detections by HB14, only one additional planet (in KOI-1151) has been discovered in any of the 60 *Kepler* systems analysed by BL13 – indicating the advantages of such predictions while searching for new planets. Completeness is an important issue (e.g. Figs 7 and 10). Some large fraction of our predictions will not be detected because the planets in this fraction are likely to be too small to produce SNR above some chosen detection threshold. Additionally, the predicted planets may have inclinations and semimajor axes too large to transit their star as seen from Earth. All new candidate detections based on the predictions of BL13 are approximately Earth-sized or smaller (Table 1).
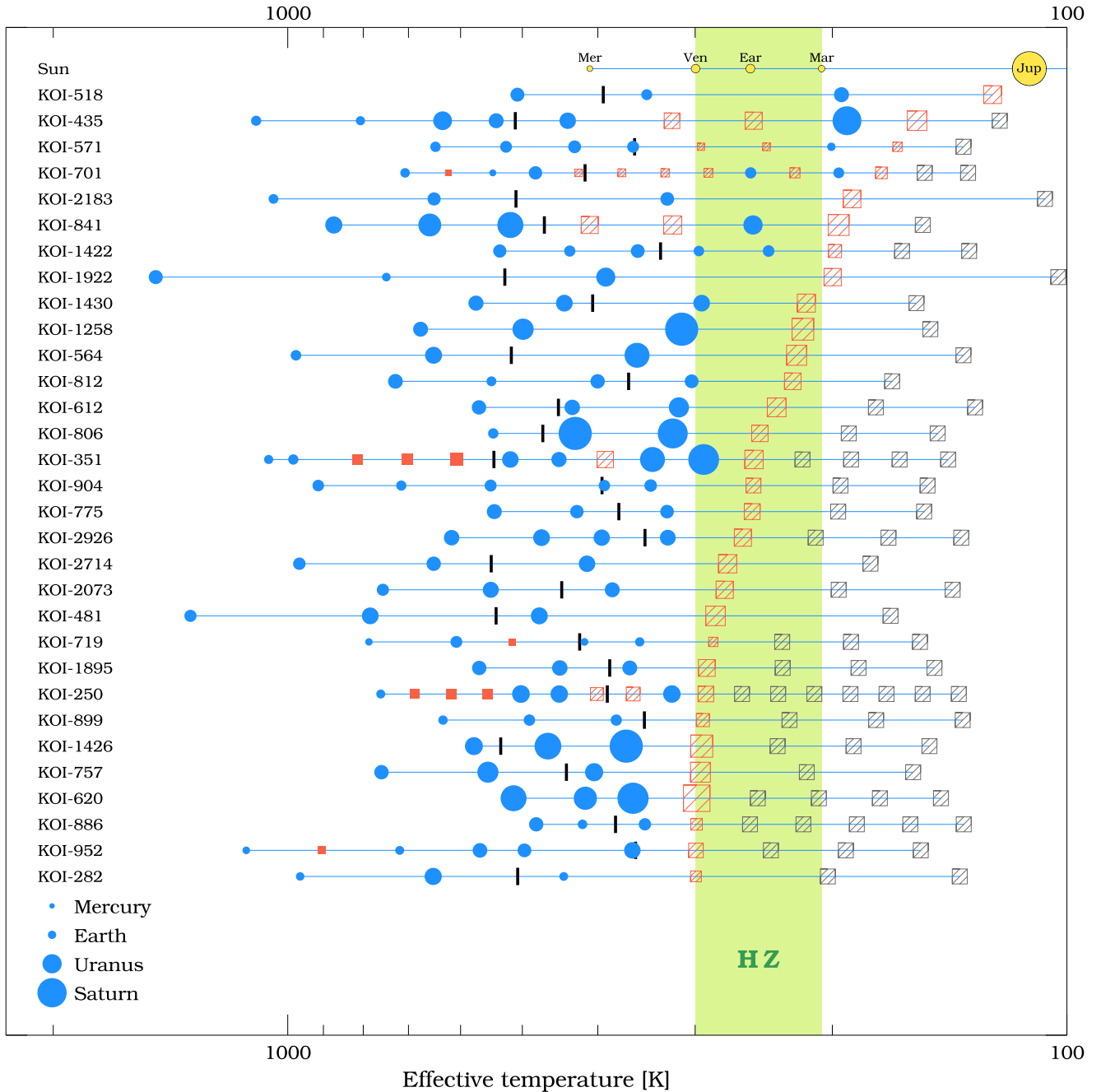
Figure 14. The effective temperatures of planets within the 31 systems from our sample which extend out to the green habitable zone (HZ) after our planet predictions are made. For the purpose of estimating the number of HZ planets per star (see Table 2), we extrapolate additional planets (grey squares) beyond the HZ. The sizes of the red hashed squares represent the R_{max} of the predicted planet.

Table 2. The estimated number of planets per star within various 'habitable zones'.

	All planets			Rocky planets ($R \leq 1.5\,R_\oplus$)		
Sample	Mars–Venus	K13 'optimistic'	K13 'conservative'	Mars–Venus	K13 'optimistic'	K13 'conservative'
All 151 systems	2.0 ± 1.0	2.3 ± 1.2	1.5 ± 0.8	0.15	0.15	0.10
Least extrapolation[b]	1.6 ± 0.9	1.7 ± 0.8	1.3 ± 0.7	0.40	0.35	0.30

Notes. [a]K13 'optimistic' and 'conservative' habitable zones refer to the 'recent Venus' to 'early Mars' and 'runaway greenhouse' to 'maximum greenhouse' regions from Kopparapu et al. (2013), respectively.
[b]The 31 systems in the sample shown in Fig. 14 are those which need the least extrapolation (red hashed squares) to extend out to (or beyond) the green Mars–Venus HZ.
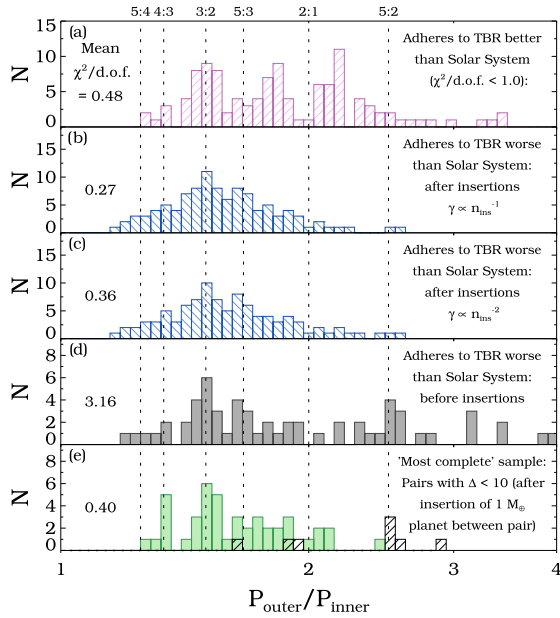
Figure 15. The period ratios of adjacent-planet pairs in our sample of *Kepler* multiples, which can be compared to fig. 4 of HB14. Panel (a) represents systems which adhere to the TB relation better than the Solar system (χ^2/d.o.f. < 1). Panel (b) represents those systems which adhere to the TB relation worse than the Solar system and where BL13 inserted planets. This panel shows the period ratios of adjacent-planet pairs after planets are inserted. Panel (c) is similar to panel (b), except that the γ value, which is used to determine the best TB relation insertion for a given system, is divided by the number of inserted planets squared. In BL13 and panel (b), γ was divided by the number of inserted planets. Panel (d) shows the period ratios between adjacent pairs of the same systems from panels (b) and (c), except before the additional planets from the predictions of BL13 have been inserted. Panel (e) represents our most complete sample and contains the systems which are more likely to be dynamically full (as defined in Section 5). The mean χ^2/d.o.f. value for each subset is shown on the left-hand side of each panel. *Kepler*'s bias towards detecting compact systems dominated by short period planets may explain why the Solar system's adjacent period pairs (black hatched histogram in panel (e) are not representative of the histogram in panel (e). The periods of predicted planets are drawn randomly from their TB relation predicted Gaussian distributions (Tables C11 and C12).
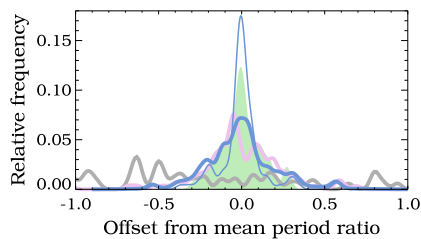
Figure 16. Each system has a mean value for the adjacent-planet period ratios within that system. This figure shows the distribution of the period ratios, offset from the mean period ratio of the system. The colours of the distributions correspond to subsets in Fig. 15. The green distribution is from the 'most complete sample' in panel (e) and is our best estimate of what a distribution should look like if an appropriate number of planets have been inserted. The grey distribution indicates that the sampling of these systems is highly incomplete. The thick and thin blue lines represent panel (c) in two different ways. The thick blue line uses planet periods drawn randomly from a normal distribution centred on the periods predicted by the TB relation, with the width set to the uncertainty in the period predictions (Tables C11 and C12). The thin blue line uses periods at their exact predicted value.

For a new sample of *Kepler* multiple-exoplanet systems containing at least three planets, we computed invariable plane inclinations and assumed a Gaussian opening angle of coplanarity of $\sigma_{\Delta\theta} = 1°5$. For each of these systems, we applied an updated generalized TB relation, developed in BL13, resulting in 228 predictions in 151 systems.

We emphasize the planet predictions which have a high geometric probability to transit, $P_{\text{trans}} \geq 0.55$ (Fig. 8). This subset of predictions has 77 predicted planets in 40 systems. We expect the detection rate in this subset to be a factor of $\sim$3 higher than the detection rate of the BL13 predictions. From the 40 systems with planet predictions in this sample, 24 appeared in BL13. These predictions have been updated and reprioritized. We have ordered our list of predicted planets based on each planet's geometric probability to transit (Tables C11 and C12). Our new prioritized predictions should help ongoing planet detection efforts in *Kepler* multiplanet systems.

ACKNOWLEDGEMENTS

REFERENCES

Ballard S., Johnson J. A., 2014, ApJ, preprint (arXiv:1410.4192)
Barnes R., Raymond S. N., 2004, ApJ, 617, 569
Bovaird T., Lineweaver C. H., 2013, MNRAS, 435, 1126
Christiansen J. L. et al., 2012, PASP, 124, 1279
Dong S., Zhu Z., 2013, ApJ, 778, 53
Dressing C. D., Charbonneau D., 2013, ApJ, 767, 95
Fabrycky D. C., Winn J. N., 2009, ApJ, 696, 1230
Fabrycky D. C. et al., 2014, ApJ, 790, 146
Fang J., Margot J.-L., 2012, ApJ, 761, 92
Fang J., Margot J.-L., 2013, ApJ, 767, 115
Figueira P. et al., 2012, A&A, 541, A139
Foreman-Mackey D., Hogg D. W., Morton T. D., 2014, ApJ, 795, 64
Fressin F. et al., 2013, ApJ, 766, 81
Gladman B., 1993, Icarus, 106, 247
Hayes W., Tremaine S., 1998, Icarus, 135, 549
Howard A. W. et al., 2012, ApJS, 201, 15
Huang C. X., Bakos G. A., 2014, MNRAS, 681, 674 (HB14)
Jaki S. L., 1972, Am. J. Phys., 40, 1014
Johansen A., Davies M. B., Church R. P., Holmelin V., 2012, ApJ, 758, 39
Kopparapu R. K. et al., 2013, ApJ, 765, 131
Kovács G., Bakos G., 2005, preprint (astro-ph/0508081)
Lillo-Box J., Barrado D., Bouy H., 2014, A&A, 556, A103
Lissauer J. J. et al., 2011, ApJS, 197, 8
Morton T. D., Swift J., 2014, ApJ, 791, 10
Petigura E. A., Howard A. W., Marcy G. W., 2013a, Proc. Natl. Acad. Sci., 110, 19273
Petigura E. A., Marcy G. W., Howard A., 2013b, ApJ, 770, 69
Rogers L. A., 2014, ApJ, preprint (arXiv:1407.4457)
Seager S., Mallén-Ornelas G., 2003, ApJ, 585, 1038
Silburt A., Gaidos E., Wu Y., 2015, ApJ, 799, 180
Souami D., Souchay J., 2012, A&A, 543, A133
Steffen J. H., Hwang J. A., 2014, MNRAS preprint (arXiv:1409.3320)
Tremaine S., Dong S., 2012, AJ, 143, 94
Watson G. S., 1982, J. Appl. Probab., 19, 265
Weissbein A., Steinberg E., 2012, preprint (arXiv:1203.6072)
Winn J. N., Fabrycky D. C., 2014, ARA&A, preprint (arXiv:1410.4199)
Wolfgang A., Lopez E., 2014, ApJ, preprint (arXiv:1409.2982)

APPENDIX A: ESTIMATION OF THE INVARIABLE PLANE OF EXOPLANET SYSTEMS

A1 Coordinate system

In Fig. 1(a) and this appendix, we set up and explain the coordinate system used in our analysis. The invariable plane of a planetary system can be defined as the plane passing through the barycentre of the system and is perpendicular to the sum $\langle L \rangle$, of all planets in the system:

$$\langle L \rangle = \sum_j L_j, \tag{A1}$$

where $L_j = (L_x, L_y, L_z)$ is the orbital angular momentum of the jth planet. One can introduce a coordinate system in which the x-axis points from the system to the observer (Fig. 1a). With an x-axis established, we are free to choose the direction of the z-axis. For example, consider the vector L_j in Fig. 1(a). If we choose a variety of z'-axes, all perpendicular to our x-axis, then independent of the z'-axis, the quantity $\sqrt{L_{y'}^2 + L_{z'}^2}$ is a constant. Thus, without loss of generality, we could choose a z'-axis such that $L_{y'} = 0$. In Fig. 1(a), we have chosen the z-axis such that the sum of the y-components of the angular momenta of all the planets, is zero:

$$\langle L \rangle = \sum_j L_j = (\langle L \rangle_x, \ 0, \ \langle L \rangle_z). \tag{A2}$$

In other words we have choosen the z-axis such that the vector defining the invariable plane, $\langle L \rangle$, is in the x–z plane. We define the plane perpendicular to this vector as the invariable plane of the system.

The angular separation between L_j and $\langle L \rangle$ is ϕ_j. ϕ_j is a positive-valued random variable and can be well represented by a Rayleigh distribution of mode σ_ϕ (Fabrycky & Winn 2009). For the jth planet, L_j is the projection of L_j on to the x–z plane. The angle between L_j and the z-axis is θ_j. The angle between $\langle L \rangle$ and the z-axis is $\langle \theta \rangle$, where

$$\langle \theta \rangle = \frac{\sum_j \theta_j L_j}{\sum L_j}. \tag{A3}$$

The angular separation in the x–z plane between L_j and $\langle L \rangle$ is $\Delta\theta_j$. In the x–z plane, we then have the relation (Fig. 1a),

$$\langle \theta \rangle + \Delta\theta_j = \theta_j, \tag{A4}$$

where $\Delta\theta_j$ is a normally distributed variable centred around $\langle \theta \rangle$ with a mean of 0. In other words, $\Delta\theta_j$ can be positive or negative. A positive definite variable such as ϕ_j is Rayleigh distributed if it can be described as the sum of the squares of two independent normally distributed variables (Watson 1982), i.e. $\phi_j = \sqrt{\Delta\theta_j^2 + \Delta\theta_{j,(y-z)}^2}$, where $\Delta\theta_{j,(y-z)}$ is the unobservable component of ϕ_j in the y–z plane perpendicular to $\Delta\theta_j$ (see Fig. 1a). From this relationship, the Gaussian distribution of $\Delta\theta_j$ has a standard deviation equal to the mode of the Rayleigh distribution of ϕ_j: $\sigma_{\Delta\theta} = \sigma_\phi$.

We can illustrate the meaning of the phrase 'mutual inclination' used in the literature (e.g. Fabrycky et al. 2014). For example, in Fig. 1(a), imagine adding the angular momentum vector L_m of another planet. And projecting this vector on to the x–z plane and call the projection L_m (just as we projected L_j into L_j). Now we can define two 'mutual inclinations' between the orbital planes of these two planets. ψ_{3D} is the angle between L_j and L_m and ψ is the angle in the x–z plane between L_j and L_m (i.e. $|\Delta\theta_j - \Delta\theta_m|$).

Since both $\Delta\theta_j$ and $\Delta\theta_m$ are Gaussian distributed with mean $\mu = 0$, their difference $\Delta\theta_j - \Delta\theta_m$ is Gaussian distributed with $\sigma_{(\Delta\theta_j - \Delta\theta_m)} = \sqrt{\sigma_{\Delta\theta_j}^2 + \sigma_{\Delta\theta_m}^2} = \sqrt{2}\sigma_{\Delta\theta}$ and $\mu_{(\Delta\theta_j - \Delta\theta_m)} = 0$. Hence $\psi = |\Delta\theta_j - \Delta\theta_m|$ is a positive-definite half-normal Gaussian with mean $\mu_\psi = \sqrt{2/\pi} \ \sigma_{(\Delta\theta_j - \Delta\theta_m)} = \frac{2}{\sqrt{\pi}}\sigma_{\Delta\theta}$.

For ψ_{3D}, the angle between L_j and L_m, we have

$$\psi_{3D} = \sqrt{(\Delta\theta_j - \Delta\theta_m)^2 + (\Delta\theta_{j,(y-z)} - \Delta\theta_{m,(y-z)})^2}. \tag{A5}$$

From above, $(\Delta\theta_j - \Delta\theta_m)$ is Gaussian distributed with $\sigma_{(\Delta\theta_j - \Delta\theta_m)} = \sqrt{2}\sigma_{\Delta\theta}$. Since we expect $\sigma_{(\Delta\theta_{j,(y-z)} - \Delta\theta_{m,(y-z)})} = \sigma_{(\Delta\theta_j - \Delta\theta_m)}$, ψ_{3D} is Rayleigh distributed with mode σ_i (reported in Table A1). That is, $\sigma_{\psi_{3D}} = \sigma_i = \sqrt{2} \ \sigma_{\Delta\theta}$. The mean of the Rayleigh distribution of ψ_{3D} is $\mu_{\psi_{3D}} = \sqrt{\pi} \ \sigma_{\Delta\theta}$. On average we will have $\mu_{\psi_{3D}}/\mu_\psi = \frac{\pi}{2}$.

A2 Exoplanet invariable planes: permuting planet inclinations

An N-planet system has N different values of θ_j (see Fig. 1). Since observations are only sensitive to $|\theta_j|$, we do not know whether

Table A1. Comparison of exoplanet coplanarity studies.

Reference	i distribution	Observables	Mode[a] of Rayleigh distributed mutual inclinations	Sample (quarter, multiplicity)
Lissauer et al. (2011)	Rayleigh	N_p[b]	$\sigma_i \sim 2°0$	*Kepler* (Q2, 1–6)
Tremaine & Dong (2012)	Fisher	N_p	σ_i[c] $< 4°0$	RV & *Kepler* (Q2, 1–6)
Figueira et al. (2012)	Rayleigh	N_p	σ_i[d] $\sim 1°4$	HARPS & *Kepler* (Q2, 1–3)
Fang & Margot (2012)	Rayleigh, R of R	N_p, ξ[e]	σ_i[c] $\sim 1°4$	*Kepler* (Q6, 1–6)
Johansen et al. (2012)	Uniform i + rotation[f]	N_p	$\sigma_i < 3°5$	*Kepler* (Q6, 1–3)
Weissbein & Steinberg (2012)	Rayleigh	N_p	No fit	*Kepler* (Q6, 1–6)
Fabrycky et al. (2014)	Rayleigh	N_p, ξ	$\sigma_i \sim 1°8$	*Kepler* (Q6, 1–6)
Ballard & Johnson (2014)	Rayleigh	N_p	$\sigma_i = 2°0^{+4°0}_{-2°0}$	*Kepler* M-dwarfs (Q16, 2–5)

Notes. [a]The mode σ_i is equal to the $\sigma_{\psi_{3D}}$ discussed at the end of Appendix A1. Thus, $\sigma_i = \sigma_{\psi_{3D}} = \sqrt{2} \ \sigma_{\Delta\theta}$. Assuming $\sigma_{\Delta\theta} = 1°5$ is equivalent to assuming $\sigma_i = 2°1$.
[b]N_p is the multiplicity vector for the numbers of observed n-planet systems, i.e. N_p = (# of one-planet systems, # of two-planet systems, # of three-planet systems, ...).
[c]Converted from the mean μ of the mutual inclination Rayleigh distribution: $\sigma_i = \sqrt{2/\pi} \ \mu$.
[d]Converted from Rayleigh distribution relative to the invariable plane: $\sigma_i = \sqrt{2} \ \sigma_{\Delta\theta}$.
[e]ξ is the normalized transit duration ratio as given in equation 11 of Fang & Margot (2012).
[f]Each planet is given a random uniform inclination between $0°$ and $5°$. This orbital plane is then rotated uniformly between 0 and 2π to give a random longitude of ascending node.

we are dealing with positive or negative angles. To model this uncertainty, we analyse the 2^{N-1} unique sets of permutations for positive and negative θ_j values. For example, in a four-planet system consider the planet with the largest angular momentum. We set our coordinate system by assuming its inclination i is less than $90°$. We do not know whether the i values of the other three planets are on the same side or the opposite side of $90°$. The permutations of the $+1$s and -1s in equation (A6) represent this uncertainty. There will be $k_{max} = 2^3 = 8$ sets of permutations for the θ_j of the remaining three planets, defined by $\theta_j \mathbf{M}_{j,k}$ where $\mathbf{M}_{j,k}$ is the permutation matrix,

$$\mathbf{M}_{j,k} = \begin{bmatrix} 1 & 1 & 1 \\ 1 & 1 & -1 \\ 1 & -1 & 1 \\ 1 & -1 & -1 \\ -1 & 1 & 1 \\ -1 & 1 & -1 \\ -1 & -1 & 1 \\ -1 & -1 & -1 \end{bmatrix}. \tag{A6}$$

For each permutation k, we compute a notional invariant plane, by taking the angular-momentum-weighted average of the permuted angles (compare equation A3):

$$\langle\theta\rangle_k = \frac{\sum L_j \theta_j \mathbf{M}_{j,k}}{\sum L_j}, \tag{A7}$$

which yields eight unique values of $\langle\theta\rangle_k$, each consistent with the b_j, θ_j and i_j values from the transit light curves (see equations 1–3). For each of these $\langle\theta\rangle_k$, we compute a proxy for coplanarity which is the mean of the angular-momentum-weighted angle of the orbital planes around the notional invariant plane:

$$\sigma_{\langle\Delta\theta\rangle_k} = \frac{\sum L_j |\langle\theta\rangle_k - \theta_j \mathbf{M}_{j,k}|}{\sum L_j}. \tag{A8}$$
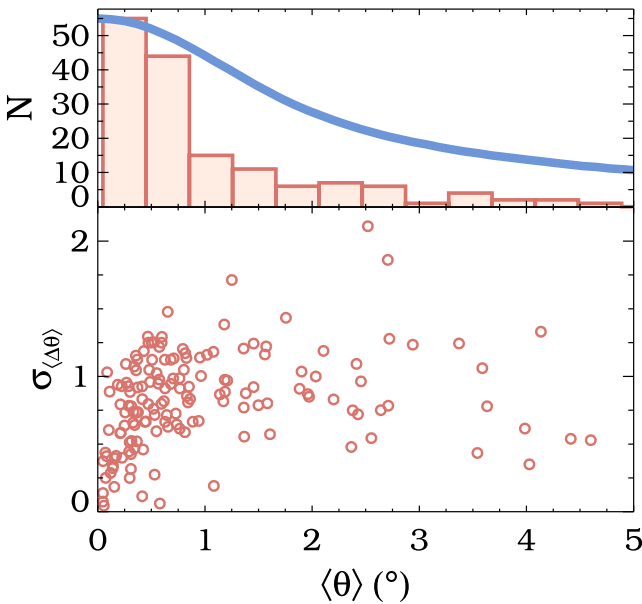
Figure A1. Top panel: the red histogram represents the final $\langle\theta\rangle$ angles for the systems in our sample. The blue line represents the normalized area out to a_{crit} as a function of $\langle\theta\rangle$ (equation B5). The bottom panel shows the dispersion for our *Kepler* multiples, about the calculated $\langle\theta\rangle$ value for each system. The smaller values of $\sigma_{\langle\Delta\theta\rangle}$ at $\langle\theta\rangle \sim 0°$ are probably due to the overrepresentation of $i = 90°$ in the *Kepler* data.

The smaller the value of $\sigma_{\langle\Delta\theta\rangle_k}$, the more coplanar that permutation set is. This permutation procedure is most appropriate when the system is close to edge-on since in this case the various planets are equally likely to have actual inclinations on either side of $90°$. By contrast, when $\langle\theta\rangle$ is large, these permutations exaggerate the uncertainty since most planets are likely to be on the same side of $90°$ as the dominant planet. Thus, using this method, close-to-edge-on systems with $\langle\theta\rangle \lesssim 0°.5$ will yield the smallest and more appropriate dispersions which we find to be in the range: $0° \lesssim \sigma_{\langle\Delta\theta\rangle_k} \lesssim 1°.5$. Since the coplanarity of a system should not depend on the angle to the observer, the values of $\sigma_{\langle\Delta\theta\rangle_k}$ should not depend on $\langle\theta\rangle$. We find that this condition can best be met when we reject permutations which yield values of $\sigma_{\langle\Delta\theta\rangle_k}$ less than $0°.4$ and greater than $1°.5$. (see Fig. A1). When no permutations for a given system meet this criteria, we select the single permutation which is closest to this range. Since the sign of $\langle\theta\rangle$ is not important, when more than one permutation meets this criterion, we estimate $\langle\theta\rangle$ by taking the median of the absolute values of the $\langle\theta\rangle_k$ for which $0°.4 \lesssim \sigma_{\langle\Delta\theta\rangle_k} \lesssim 1°.5$. These permutations are used in Figs 11–13, where the most probable inclination ambiguities are indicated by two blue planets at the same semimajor axis, one above and one below the $i = 90$ dashed horizontal line.

APPENDIX B: CALCULATING THE GEOMETRIC PROBABILITY TO TRANSIT: P_{trans}

We assume $\sigma_{\Delta\theta} = 1°.5$ is constant over all systems (Section 1.1), such that the geometric probability for the jth planet to transit is the fraction of a Gaussian-weighted opening angle within the transit region, where the standard deviation of the Gaussian is $\sigma_j = a_j \sigma_{\Delta\theta}$ (Fig. B1 and equation B1)

$$P_{trans}(\langle\theta\rangle, a_j) = \frac{1}{\sigma_j \sqrt{2\pi}} \int_{u_1}^{u_2} e^{-\frac{u^2}{2\sigma_j^2}} \, du, \tag{B1}$$
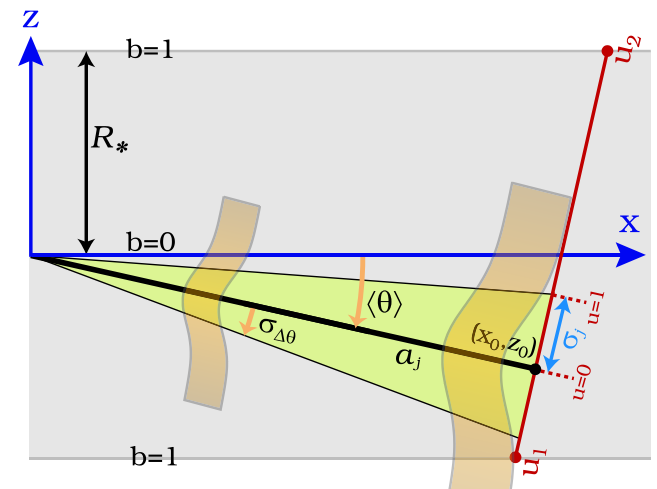
Figure B1. Illustration of the variables required to calculate P_{trans} (equation B1), the fraction of a Gaussian within the transit region ($b \lesssim 1$). We assume that a planet with semimajor axis a_j, in a system whose invariable plane is the thick line, will have a position $\Delta\theta_j$, whose probability will be described by a normal distribution along the red line perpendicular to the invariant plane. The integration variable u of equation (B1) is along this perpendicular red line. The mean of the Gaussian is at the point (x_o, z_o) where $u = 0$. The standard deviation $\sigma_j = a_j \sigma_{\Delta\theta}$ is also the half-width of the green region at a distance a_j from the host star.

where the integration limits u_1 and u_2 are defined by (see Fig. B1)

$$u_1 = \frac{R_* + z_o}{\cos\langle\theta\rangle} \tag{B2}$$

$$u_2 = \frac{R_* - z_o}{\cos\langle\theta\rangle} \tag{B3}$$

$$z_0 = -a_j \sin\langle\theta\rangle \tag{B4}$$

with the axes in Fig. B1 being the same as in panel (b) of Fig. 1, we have $z_o < 0$. And since $\langle\theta\rangle \sim 0$, we have $\cos\langle\theta\rangle \sim 1$.

In the panels of Figs 11–13, the green area is a function of the $\langle\theta\rangle$ of the system. We can integrate P_{trans} to get the size of the green area that is closer to the host star than a_{crit}. This yields an area that is an estimate of the amount of parameter space in which planets can transit:

$$\text{Area}(\langle\theta\rangle) = \int_0^{a_{\text{crit}}(\langle\theta\rangle)} P_{\text{trans}}\, da. \tag{B5}$$

In the top panel of Fig. A1, the blue curve is a normalized version of equation (B5) and represents the statistical expectation of the number of systems as a function of $\langle\theta\rangle$ (ignoring detection biases). The histogram shows the values we have obtained.

APPENDIX C: TABLES OF PLANET PREDICTIONS

Table C1. 77 planet predictions with a high geometric probability to transit ($P_{\text{trans}} \geq 0.55$) in 40 *Kepler* systems.

System	Number inserted	γ	$\Delta\gamma^a$	$\left(\frac{\chi^2}{\text{d.o.f.}}\right)_i$	$\left(\frac{\chi^2}{\text{d.o.f.}}\right)_f$	Inserted planet #	Period (d)	a (au)	$R_{\max}{}^b$ ($R_\oplus$)	T_{eff} (K)	P_{trans}
KOI-1198	2	2.2	0.3	7.19	0.74	1	2.1 ± 0.4	0.03	1.3	1642	1.00
						2	4.3 ± 0.7	0.06	1.5	1297	1.00
KOI-1955	4	3.4	0.2	10.23	0.19	1	2.6 ± 0.3	0.04	0.9	1568	1.00
						2	4.1 ± 0.5	0.05	1.0	1347	1.00
						3	6.4 ± 0.7	0.07	1.2	1157	0.99
						4	10.1 ± 1.1	0.10	1.3	994	0.94
KOI-1082	2	23.0	5.0	5.02	0.06	1	1.8 ± 0.2	0.03	1.0	1184	1.00
						2	2.8 ± 0.3	0.04	1.1	1029	1.00
						3 E^c	14.7 ± 1.4	0.11	1.6	588	0.72
KOI-952	1	2.2	5.2	2.36	0.76	1	1.5 ± 0.3	0.02	0.9	904	1.00
KOI-500	2	7.6	1.9	5.47	0.18	1	1.5 ± 0.2	0.02	1.2	1091	1.00
						2	2.1 ± 0.2	0.03	1.3	960	1.00
KOI-4032	2	0.9	1.9	1.20	0.27	1	3.4 ± 0.2	0.04	0.8	1347	1.00
						2	4.5 ± 0.2	0.05	0.9	1224	0.99
						3 E	6.9 ± 0.3	0.07	1.0	1061	0.91
KOI-707	1	3.2	2.2	3.69	0.90	1	8.9 ± 0.8	0.09	2.0	1162	1.00
KOI-1336	2	1.3	65.6	1.07	0.19	1	6.7 ± 0.7	0.07	1.7	1053	0.98
						2	25.1 ± 2.5	0.17	2.4	679	0.64
KOI-2859	1	10.2	−1.0	1.69	0.16	1	2.4 ± 0.1	0.03	0.6	1242	0.98
KOI-250	5	0.7	1.1	2.26	0.14	1	4.8 ± 0.4	0.05	1.2	686	0.96
						2	6.6 ± 0.6	0.06	1.3	616	0.91
						3	9.2 ± 0.8	0.07	1.4	553	0.83
KOI-168	0	–	–	0.14	–	1 E	22.6 ± 1.2	0.17	2.6	909	0.95
						2 E	33.2 ± 1.4	0.21	2.9	800	0.87
						3 E	48.6 ± 1.7	0.28	3.2	704	0.76
						4 E	71.3 ± 2.2	0.36	3.5	620	0.64
KOI-2585	0	–	–	0.55	–	1 E	14.8 ± 0.7	0.12	1.1	967	0.95
						2 E	20.7 ± 0.8	0.15	1.2	865	0.87
						3 E	28.9 ± 0.9	0.19	1.3	774	0.78
						4 E	40.4 ± 1.1	0.24	1.4	692	0.67
						5 E	56.4 ± 1.3	0.30	1.6	619	0.57
KOI-1052	2	115.4	40.4	1.36	0.01	1	10.8 ± 1.2	0.10	1.6	909	0.94
						2	27.1 ± 2.8	0.18	2.0	669	0.69
KOI-505	3	1.6	0.1	8.20	0.56	1	21.9 ± 2.5	0.15	4.5	788	0.92
						2	34.7 ± 3.9	0.20	5.1	676	0.78
						3	55 ± 7	0.27	5.7	580	0.62
KOI-1831	1	1.3	0.2	2.54	1.11	1	8.2 ± 1.1	0.08	0.9	739	0.91
KOI-248	1	18.3	80.8	2.48	0.13	1	4.2 ± 0.5	0.04	1.4	633	0.89
KOI-880	1	4.0	22.4	1.35	0.28	1	11.8 ± 2.0	0.10	2.1	761	0.89
KOI-1567	2	5.9	44.8	1.51	0.07	1	11.4 ± 1.2	0.10	2.0	668	0.89
						2	28.0 ± 2.9	0.18	2.5	494	0.62
KOI-1952	2	85.6	16.6	3.26	0.01	1	12.1 ± 1.2	0.10	1.5	828	0.87
						2	18.3 ± 1.8	0.14	1.6	720	0.75
KOI-351	4	0.5	1.0	5.78	0.65	1	15.4 ± 1.7	0.13	1.4	813	0.87
						2	23.9 ± 2.5	0.17	1.6	702	0.74
						3	37.1 ± 3.9	0.23	1.8	607	0.60

Table C1 – *continued*

System	Number inserted	γ	$\Delta\gamma^a$	$\left(\frac{\chi^2}{\text{d.o.f.}}\right)_i$	$\left(\frac{\chi^2}{\text{d.o.f.}}\right)_f$	Inserted planet #	Period (d)	a (au)	$R_{\max}{}^b$ ($R_\oplus$)	T_{eff} (K)	P_{trans}
KOI-701	6	18.0	7.4	4.04	0.01	1	8.4 ± 0.8	0.07	0.6	621	0.87
KOI-1306	1	5.7	0.4	4.12	0.62	1	13.7 ± 2.1	0.11	1.5	756	0.85
KOI-2722	0	–	–	0.54	–	1 E	23.4 ± 1.5	0.17	1.4	774	0.78
						2 E	33.0 ± 1.8	0.21	1.5	690	0.67
						3 E	46.5 ± 2.3	0.27	1.6	615	0.56
KOI-1358	0	–	–	0.01	–	1 E	13.6 ± 1.0	0.10	1.6	522	0.74
						2 E	21.0 ± 1.3	0.14	1.8	451	0.60
KOI-1627	0	–	–	0.24	–	1 E	16.6 ± 1.2	0.13	1.9	586	0.73
						2 E	27.4 ± 1.5	0.17	2.1	497	0.57
KOI-1833	0	–	–	0.74	–	1 E	11.3 ± 0.6	0.08	2.0	514	0.72
						2 E	16.4 ± 0.7	0.10	2.2	455	0.60
KOI-3158	0	–	–	0.23	–	1 E	12.7 ± 0.6	0.09	0.4	566	0.71
						2 E	16.4 ± 0.7	0.11	0.4	520	0.62
KOI-2055	0	–	–	0.29	–	1 E	13.6 ± 1.0	0.11	1.3	703	0.70
						2 E	20.6 ± 1.2	0.14	1.5	612	0.56
KOI-245	3	1.0	1.3	1.56	0.17	1	16.8 ± 0.9	0.12	0.3	582	0.70
						2	26.1 ± 1.4	0.16	0.3	502	0.56
KOI-749	0	–	–	0.49	–	1 E	11.4 ± 0.6	0.10	1.5	711	0.69
						2 E	16.4 ± 0.7	0.12	1.7	630	0.57
KOI-730	0	–	–	0.33	–	1 E	27.9 ± 1.5	0.18	2.3	620	0.69
						2 E	39.0 ± 1.8	0.22	2.5	554	0.58
KOI-719	1	1.1	1.5	1.36	0.66	1	14.8 ± 2.0	0.11	0.8	514	0.69
KOI-1060	0	–	–	0.22	–	1 E	32.7 ± 2.6	0.22	2.1	703	0.68
KOI-3083	0	–	–	0.56	–	1 E	13.2 ± 0.5	0.11	0.7	751	0.66
						2 E	16.9 ± 0.5	0.13	0.7	692	0.57
KOI-156	0	–	–	0.10	–	1 E	17.9 ± 1.0	0.12	1.6	476	0.61
KOI-137	0	–	–	0.13	–	1 E	31.2 ± 3.1	0.19	3.1	539	0.60
KOI-1151	0	–	–	0.85	–	1 E	33.0 ± 2.2	0.20	1.0	564	0.59
KOI-1015	0	–	–	0.62	–	1 E	36.1 ± 3.5	0.22	2.3	590	0.58
KOI-2029	0	–	–	0.31	–	1 E	23.7 ± 1.6	0.15	0.9	514	0.56
KOI-664	0	–	–	0.06	–	1 E	40.3 ± 3.0	0.23	1.5	618	0.56

Notes. $^a\Delta\gamma = (\gamma_1 - \gamma_2)/\gamma_2$ where γ_1 and γ_2 are the highest and second highest γ values for that system, respectively (see Bovaird & Lineweaver 2013).
$^b R_{\max}$ is calculated by applying the lowest SNR of the detected planets in the system to the period of the inserted planet. See equation (7).
^{c}A planet number followed by 'E' indicates the planet is extrapolated (has a larger period than the outermost detected planet in the system).

Table C2. All 228 planet predictions in 151 systems (Table C1 1 is a high P_{trans} subset of this table).

System	Number inserted	γ	$\Delta\gamma^a$	$\left(\frac{\chi^2}{\text{d.o.f.}}\right)_i$	$\left(\frac{\chi^2}{\text{d.o.f.}}\right)_f$	Inserted planet #	Period (d)	a (au)	$R_{\max}{}^b$ ($R_\oplus$)	$T_{\text{eff}}{}^e$ (K)	$P_{\text{trans}}{}^d$
KOI-1198	2	2.2	0.3	7.19	0.74	1	2.1 ± 0.4	0.03	1.3	1642	**1.00**
						2	4.3 ± 0.7	0.06	1.5	1297	**1.00**
						3 E ^{c}	73 ± 12	0.37	3.1	505	0.41
KOI-1955	4	3.4	0.2	10.23	0.19	1	2.6 ± 0.3	0.04	0.9	1568	**1.00**
						2	4.1 ± 0.5	0.05	1.0	1347	**1.00**
						3	6.4 ± 0.7	0.07	1.2	1157	**0.99**
						4	10.1 ± 1.1	0.10	1.3	994	**0.94**
						5 E	62 ± 7	0.33	2.0	541	0.42
KOI-1082	2	23.0	5.0	5.02	0.06	1	1.8 ± 0.2	0.03	1.0	1184	**1.00**
						2	2.8 ± 0.3	0.04	1.1	1029	**1.00**
						3 E	14.7 ± 1.4	0.11	1.6	588	0.72
KOI-952	1	2.2	5.2	2.36	0.76	1	1.5 ± 0.3	0.02	0.9	904	**1.00**
						2 E	40.0 ± 6.2	0.19	2.1	**299**	0.36
KOI-500	2	7.6	1.9	5.47	0.18	1	1.5 ± 0.2	0.02	1.2	1091	**1.00**
						2	2.1 ± 0.2	0.03	1.3	960	**1.00**
						3 E	14.5 ± 1.3	0.10	2.2	506	0.50

Table C2 – *continued*

System	Number inserted	γ	$\Delta\gamma^a$	$\left(\frac{\chi^2}{\text{d.o.f.}}\right)_i$	$\left(\frac{\chi^2}{\text{d.o.f.}}\right)_f$	Inserted planet #	Period (d)	a (au)	$R_{\max}^{\,b}$ ($R_\oplus$)	$T_{\text{eff}}^{\,e}$ (K)	$P_{\text{trans}}^{\,d}$
KOI-4032	2	0.9	1.9	1.20	0.27	1	3.4 ± 0.2	0.04	0.8	1347	**1.00**
						2	4.5 ± 0.2	0.05	0.9	1224	**0.99**
						3 E	6.9 ± 0.3	0.07	1.0	1061	0.91
KOI-707	1	3.2	2.2	3.69	0.90	1	8.9 ± 0.8	0.09	2.0	1162	**1.00**
						2 E	68 ± 7	0.35	3.3	590	0.50
KOI-1336	2	1.3	65.6	1.07	0.19	1	6.7 ± 0.7	0.07	1.7	1053	**0.98**
						2	25.1 ± 2.5	0.17	2.4	679	**0.64**
						3 E	60 ± 6	0.31	3.0	507	0.39
KOI-2859	1	10.2	−1.0	1.69	0.16	1	2.4 ± 0.1	0.03	0.6	1242	**0.98**
						2 E	5.1 ± 0.3	0.05	0.8	967	0.54
KOI-250	5	0.7	1.1	2.26	0.14	1	4.8 ± 0.4	0.05	1.2	686	**0.96**
						2	6.6 ± 0.6	0.06	1.3	616	**0.91**
						3	9.2 ± 0.8	0.07	1.4	553	**0.83**
						4	24.1 ± 1.9	0.14	1.8	401	0.53
						5	33.2 ± 2.6	0.17	2.0	360	0.44
						6 E	63.3 ± 5.0	0.27	2.3	**290**	0.29
KOI-168	0	–	–	0.14	–	1 E	22.6 ± 1.2	0.17	2.6	909	**0.95**
						2 E	33.2 ± 1.4	0.21	2.9	800	**0.87**
						3 E	48.6 ± 1.7	0.28	3.2	704	**0.76**
						4 E	71.3 ± 2.2	0.36	3.5	620	**0.64**
						5 E	104.5 ± 2.7	0.46	3.8	546	0.52
KOI-2585	0	–	–	0.55	–	1 E	14.8 ± 0.7	0.12	1.1	967	**0.95**
						2 E	20.7 ± 0.8	0.15	1.2	865	**0.87**
						3 E	28.9 ± 0.9	0.19	1.3	774	**0.78**
						4 E	40.4 ± 1.1	0.24	1.4	692	**0.67**
						5 E	56.4 ± 1.3	0.30	1.6	619	**0.57**
KOI-1052	2	115.4	40.4	1.36	0.01	1	10.8 ± 1.2	0.10	1.6	909	**0.94**
						2	27.1 ± 2.8	0.18	2.0	669	**0.69**
						3 E	110 ± 20	0.46	2.8	423	0.31
KOI-505	3	1.6	0.1	8.20	0.56	1	21.9 ± 2.5	0.15	4.5	788	**0.92**
						2	34.7 ± 3.9	0.20	5.1	676	**0.78**
						3	55 ± 7	0.27	5.7	580	**0.62**
						4 E	140 ± 20	0.51	7.2	426	0.36
KOI-1831	1	1.3	0.2	2.54	1.11	1	8.2 ± 1.1	0.08	0.9	739	**0.91**
						2 E	100 ± 20	0.41	1.7	316	0.25
KOI-248	1	18.3	80.8	2.48	0.13	1	4.2 ± 0.5	0.04	1.4	633	**0.89**
						2 E	30.1 ± 3.3	0.16	2.2	329	0.30
KOI-880	1	4.0	22.4	1.35	0.28	1	11.8 ± 2.0	0.10	2.1	761	**0.89**
						2 E	120 ± 20	0.45	3.7	354	0.27
KOI-1567	2	5.9	44.8	1.51	0.07	1	11.4 ± 1.2	0.10	2.0	668	**0.89**
						2	28.0 ± 2.9	0.18	2.5	494	**0.62**
						3 E	69 ± 8	0.32	3.1	366	0.37
KOI-1952	2	85.6	16.6	3.26	0.01	1	12.1 ± 1.2	0.10	1.5	828	**0.87**
						2	18.3 ± 1.8	0.14	1.6	720	**0.75**
						3 E	64 ± 7	0.31	2.2	474	0.38
KOI-351	4	0.5	1.0	5.78	0.65	1	15.4 ± 1.7	0.13	1.4	813	**0.87**
						2	23.9 ± 2.5	0.17	1.6	702	**0.74**
						3	37.1 ± 3.9	0.23	1.8	607	**0.60**
						4	140 ± 20	0.54	2.4	391	0.27
						5 E	520 ± 60	1.31	3.4	**252**	0.12
KOI-701	6	18.0	7.4	4.04	0.01	1	8.4 ± 0.8	0.07	0.6	621	**0.87**
						2	26.6 ± 2.6	0.15	0.8	423	0.52
						3	39.1 ± 3.7	0.19	0.9	372	0.41
						4	57 ± 6	0.25	1.0	327	0.33
						5	84 ± 8	0.32	1.1	**288**	0.25
						6	180 ± 20	0.54	1.3	**223**	0.15
						7 E	390 ± 40	0.90	1.6	172	0.09
KOI-1306	1	5.7	0.4	4.12	0.62	1	13.7 ± 2.1	0.11	1.5	756	**0.85**
						2 E	55 ± 9	0.28	2.1	476	0.43
KOI-2722	0	–	–	0.54	–	1 E	23.4 ± 1.5	0.17	1.4	774	**0.78**
						2 E	33.0 ± 1.8	0.21	1.5	690	**0.67**
						3 E	46.5 ± 2.3	0.27	1.6	615	**0.56**

Table C2 – *continued*

System	Number inserted	γ	$\Delta\gamma^a$	$\left(\frac{\chi^2}{\text{d.o.f.}}\right)_i$	$\left(\frac{\chi^2}{\text{d.o.f.}}\right)_f$	Inserted planet #	Period (d)	a (au)	R_{max}^b ($R_\oplus$)	T_{eff}^e (K)	P_{trans}^d
KOI-1358	0	–	–	0.01	–	1 E	13.6 ± 1.0	0.10	1.6	522	**0.74**
						2 E	21.0 ± 1.3	0.14	1.8	451	**0.60**
KOI-1627	0	–	–	0.24	–	1 E	16.6 ± 1.2	0.13	1.9	586	**0.73**
						2 E	27.4 ± 1.5	0.17	2.1	497	**0.57**
KOI-1833	0	–	–	0.74	–	1 E	11.3 ± 0.6	0.08	2.0	514	**0.72**
						2 E	16.4 ± 0.7	0.10	2.2	455	**0.60**
KOI-3158	0	–	–	0.23	–	1 E	12.7 ± 0.6	0.09	0.4	566	**0.71**
						2 E	16.4 ± 0.7	0.11	0.4	520	**0.62**
						3 E	21.1 ± 0.8	0.13	0.5	478	**0.55**
KOI-2055	0	–	–	0.29	–	1 E	13.6 ± 1.0	0.11	1.3	703	**0.70**
						2 E	20.6 ± 1.2	0.14	1.5	612	**0.56**
KOI-245	3	1.0	1.3	1.56	0.17	1	16.8 ± 0.9	0.12	0.3	582	**0.70**
						2	26.1 ± 1.4	0.16	0.3	502	**0.56**
						3	32.6 ± 1.7	0.18	0.3	467	0.50
						4 E	63.1 ± 3.3	0.28	0.4	374	0.33
KOI-749	0	–	–	0.49	–	1 E	11.4 ± 0.6	0.10	1.5	711	**0.69**
						2 E	16.4 ± 0.7	0.12	1.7	630	**0.57**
KOI-730	0	–	–	0.33	–	1 E	27.9 ± 1.5	0.18	2.3	620	**0.69**
						2 E	39.0 ± 1.8	0.22	2.5	554	**0.58**
KOI-719	1	1.1	1.5	1.36	0.66	1	14.8 ± 2.0	0.11	0.8	514	**0.69**
						2 E	88 ± 12	0.35	1.2	**284**	0.24
KOI-1060	0	–	–	0.22	–	1 E	32.7 ± 2.6	0.22	2.1	703	**0.68**
						2 E	52.7 ± 3.5	0.30	2.3	599	0.53
KOI-3083	0	–	–	0.56	–	1 E	13.2 ± 0.5	0.11	0.7	751	**0.66**
						2 E	16.9 ± 0.5	0.13	0.7	692	**0.57**
KOI-156	0	–	–	0.10	–	1 E	17.9 ± 1.0	0.12	1.6	476	**0.61**
KOI-137	0	–	–	0.13	–	1 E	31.2 ± 3.1	0.19	3.1	539	**0.60**
KOI-1151	0	–	–	0.85	–	1 E	33.0 ± 2.2	0.20	1.0	564	**0.59**
KOI-1015	0	–	–	0.62	–	1 E	36.1 ± 3.5	0.22	2.3	590	**0.58**
KOI-2029	0	–	–	0.31	–	1 E	23.7 ± 1.6	0.15	0.9	514	**0.56**
KOI-664	0	–	–	0.06	–	1 E	40.3 ± 3.0	0.23	1.5	618	**0.56**
KOI-2693	0	–	–	0.01	–	1 E	19.1 ± 1.4	0.12	1.0	430	0.53
KOI-1590	0	–	–	0.64	–	1 E	28.7 ± 3.3	0.16	1.8	452	0.53
KOI-279	0	–	–	0.13	–	1 E	56 ± 6	0.30	1.3	586	0.53
KOI-1930	0	–	–	0.60	–	1 E	72 ± 7	0.35	2.3	541	0.52
KOI-70	1	7.4	2.9	3.51	0.42	1	39.1 ± 5.4	0.22	1.2	498	0.52
						2 E	130 ± 20	0.49	1.7	331	0.24
KOI-720	0	–	–	0.14	–	1 E	34.8 ± 3.6	0.20	2.9	477	0.51
KOI-1860	0	–	–	0.02	–	1 E	49.5 ± 5.6	0.27	1.7	512	0.49
KOI-1475	0	–	–	0.94	–	1 E	24.6 ± 3.0	0.14	1.7	377	0.48
KOI-1194	0	–	–	0.52	–	1 E	29.0 ± 2.5	0.16	1.8	374	0.47
KOI-2025	0	–	–	0.21	–	1 E	40.5 ± 2.4	0.24	2.3	647	0.47
KOI-733	0	–	–	0.22	–	1 E	35.5 ± 3.5	0.20	2.8	437	0.46
KOI-2169	0	–	–	0.87	–	1 E	7.6 ± 0.4	0.07	0.7	868	0.46
KOI-2163	0	–	–	0.06	–	1 E	46.3 ± 3.1	0.26	1.7	532	0.44
KOI-3319	0	–	–	0.01	–	1 E	45.9 ± 5.3	0.25	2.1	517	0.44
KOI-2352	0	–	–	0.28	–	1 E	20.3 ± 1.2	0.16	1.1	845	0.44
KOI-1681	0	–	–	0.15	–	1 E	12.7 ± 1.1	0.09	1.3	415	0.44
KOI-1413	0	–	–	0.14	–	1 E	56.2 ± 3.8	0.28	1.8	458	0.44
KOI-2597	0	–	–	0.13	–	1 E	17.7 ± 1.0	0.14	1.8	791	0.43
KOI-2220	0	–	–	0.19	–	1 E	19.1 ± 1.6	0.14	1.2	695	0.42
KOI-1161	0	–	–	0.18	–	1 E	21.4 ± 1.9	0.14	2.1	574	0.42
KOI-582	0	–	–	0.08	–	1 E	30.3 ± 2.3	0.18	1.8	466	0.41
KOI-82	0	–	–	0.92	–	1 E	38.3 ± 2.9	0.21	0.9	408	0.41
KOI-157	1	3.7	6.9	3.15	0.69	1	75 ± 8	0.34	2.7	439	0.41
						2 E	170 ± 20	0.60	3.4	334	0.24
KOI-864	0	–	–	0.09	–	1 E	44.0 ± 4.6	0.24	2.9	453	0.40
KOI-939	0	–	–	0.24	–	1 E	20.3 ± 2.1	0.15	1.9	640	0.40
KOI-898	0	–	–	0.08	–	1 E	39.1 ± 3.6	0.20	2.8	360	0.40
KOI-841	2	7.1	0.4	4.35	0.15	1	63 ± 11	0.31	2.7	409	0.39
						2	130 ± 30	0.51	3.3	320	0.25
						3 E	580 ± 100	1.35	4.7	196	0.09

Table C2 – *continued*

System	Number inserted	γ	$\Delta\gamma^a$	$\left(\frac{\chi^2}{\text{d.o.f.}}\right)_i$	$\left(\frac{\chi^2}{\text{d.o.f.}}\right)_f$	Inserted planet #	Period (d)	a (au)	$R_{max}{}^b$ ($R_\oplus$)	$T_{eff}{}^e$ (K)	$P_{trans}{}^d$
KOI-408	0	–	–	0.51	–	1 E	59 ± 7	0.29	2.6	461	0.39
KOI-1909	0	–	–	0.26	–	1 E	55 ± 6	0.29	1.9	500	0.38
KOI-2715	0	–	–	0.62	–	1 E	26.1 ± 2.9	0.14	3.9	379	0.38
KOI-1278	0	–	–	0.52	–	1 E	73 ± 7	0.35	2.0	455	0.38
KOI-1867	0	–	–	0.53	–	1 E	31.3 ± 3.6	0.16	1.7	323	0.37
KOI-899	0	–	–	0.01	–	1 E	33.1 ± 3.5	0.16	1.9	**293**	0.37
KOI-1589	0	–	–	0.56	–	1 E	82 ± 9	0.37	2.4	440	0.37
KOI-884	0	–	–	0.45	–	1 E	53 ± 7	0.25	2.9	362	0.37
KOI-829	0	–	–	0.07	–	1 E	76 ± 8	0.36	3.5	442	0.37
KOI-94	0	–	–	0.19	–	1 E	130 ± 20	0.55	4.2	452	0.36
KOI-2038	0	–	–	0.11	–	1 E	37.0 ± 2.3	0.21	1.8	494	0.36
KOI-1557	0	–	–	0.58	–	1 E	18.2 ± 1.9	0.12	2.0	499	0.35
KOI-571	2	19.9	5.2	4.87	0.07	1	40.9 ± 5.6	0.19	0.8	**294**	0.35
						2	73 ± 10	0.28	0.9	**242**	0.24
						3 E	230 ± 40	0.61	1.2	164	0.11
KOI-1905	0	–	–	0.01	–	1 E	72 ± 8	0.32	1.7	374	0.34
KOI-116	0	–	–	0.34	–	1 E	86 ± 10	0.38	1.3	425	0.34
KOI-2732	0	–	–	0.22	–	1 E	100 ± 20	0.44	1.3	426	0.34
KOI-665	0	–	–	0.01	–	1 E	11.2 ± 1.0	0.10	1.5	893	0.34
KOI-1931	0	–	–	0.20	–	1 E	15.2 ± 0.8	0.12	1.5	661	0.33
KOI-886	0	–	–	0.46	–	1 E	33.2 ± 2.2	0.16	1.6	**298**	0.32
KOI-1432	0	–	–	0.07	–	1 E	87 ± 13	0.38	2.0	397	0.32
KOI-945	0	–	–	0.04	–	1 E	107 ± 7	0.46	2.6	424	0.32
KOI-869	0	–	–	0.08	–	1 E	84 ± 12	0.35	3.8	349	0.31
KOI-111	0	–	–	0.03	–	1 E	110 ± 20	0.42	2.8	376	0.30
KOI-1364	0	–	–	0.41	–	1 E	34.9 ± 3.3	0.20	3.0	508	0.30
KOI-1832	0	–	–	0.03	–	1 E	110 ± 20	0.44	3.6	381	0.30
KOI-658	0	–	–	0.60	–	1 E	20.7 ± 1.8	0.15	1.4	649	0.30
KOI-1895	0	–	–	0.11	–	1 E	64 ± 6	0.27	2.6	**289**	0.30
KOI-2926	0	–	–	0.49	–	1 E	73 ± 8	0.27	2.8	**260**	0.29
KOI-1647	0	–	–	0.07	–	1 E	74 ± 9	0.34	2.0	460	0.29
KOI-941	0	–	–	0.36	–	1 E	75 ± 12	0.32	4.7	343	0.29
KOI-3741	0	–	–	0.01	–	1 E	35.3 ± 3.1	0.21	2.2	709	0.28
KOI-700	0	–	–	0.91	–	1 E	120 ± 20	0.48	2.1	388	0.28
KOI-1563	0	–	–	0.62	–	1 E	26.9 ± 2.5	0.17	3.6	491	0.28
KOI-2135	0	–	–	0.12	–	1 E	140 ± 20	0.53	1.9	414	0.28
KOI-2433	0	–	–	0.55	–	1 E	150 ± 20	0.57	2.9	395	0.28
KOI-2086	0	–	–	0.33	–	1 E	15.2 ± 0.6	0.13	2.7	933	0.27
KOI-1102	0	–	–	0.75	–	1 E	32.4 ± 2.7	0.20	2.8	630	0.27
KOI-3097	0	–	–	0.31	–	1 E	15.6 ± 0.6	0.13	1.3	1033	0.27
KOI-1445	0	–	–	0.01	–	1 E	150 ± 30	0.59	1.4	391	0.27
KOI-232	0	–	–	0.93	–	1 E	110 ± 20	0.46	2.1	391	0.26
KOI-520	0	–	–	0.18	–	1 E	110 ± 20	0.42	1.8	314	0.26
KOI-2707	0	–	–	0.29	–	1 E	110 ± 20	0.45	2.3	335	0.25
KOI-152	0	–	–	0.64	–	1 E	160 ± 20	0.60	3.6	381	0.25
KOI-1332	0	–	–	0.03	–	1 E	170 ± 30	0.63	3.8	337	0.25
KOI-2485	0	–	–	0.17	–	1 E	16.4 ± 1.2	0.12	1.8	575	0.25
KOI-877	0	–	–	0.32	–	1 E	40.0 ± 3.4	0.20	1.6	343	0.24
KOI-775	0	–	–	0.04	–	1 E	78 ± 9	0.30	2.4	**253**	0.24
KOI-757	0	–	–	0.01	–	1 E	110 ± 20	0.41	4.2	**295**	0.24
KOI-510	0	–	–	0.05	–	1 E	78 ± 11	0.34	3.5	413	0.24
KOI-117	0	–	–	0.42	–	1 E	23.3 ± 2.0	0.17	1.4	692	0.23
KOI-935	0	–	–	0.03	–	1 E	180 ± 30	0.68	4.1	374	0.23
KOI-285	0	–	–	0.04	–	1 E	94 ± 9	0.43	2.2	490	0.22
KOI-671	0	–	–	0.62	–	1 E	26.4 ± 2.0	0.17	1.5	614	0.22
KOI-834	0	–	–	0.84	–	1 E	120 ± 20	0.47	2.5	351	0.22
KOI-509	0	–	–	0.22	–	1 E	120 ± 20	0.46	2.5	334	0.22
KOI-904	0	–	–	0.93	–	1 E	100 ± 20	0.37	2.2	**252**	0.22
KOI-723	0	–	–	0.04	–	1 E	74 ± 10	0.33	4.2	357	0.22
KOI-1436	0	–	–	0.19	–	1 E	31.3 ± 3.6	0.19	2.3	555	0.21

Table C2 – *continued*

System	Number inserted	γ	$\Delta\gamma^a$	$\left(\frac{\chi^2}{\text{d.o.f.}}\right)_i$	$\left(\frac{\chi^2}{\text{d.o.f.}}\right)_f$	Inserted planet #	Period (d)	a (au)	$R_{\max}{}^b$ ($R_\oplus$)	$T_{\text{eff}}{}^e$ (K)	$P_{\text{trans}}{}^d$
KOI-435	2	1.8	0.3	6.69	0.84	1	160 ± 30	0.55	2.3	321	0.21
						2	320 ± 60	0.90	2.8	**252**	0.13
						3 E	1380 ± 250	2.35	4.0	155	0.05
KOI-2073	0	–	–	0.08	–	1 E	130 ± 20	0.46	2.8	**274**	0.20
KOI-812	0	–	–	0.04	–	1 E	110 ± 20	0.38	2.5	**224**	0.20
KOI-474	0	–	–	0.54	–	1 E	230 ± 40	0.77	3.8	336	0.20
KOI-907	0	–	–	0.91	–	1 E	250 ± 50	0.76	4.5	309	0.19
KOI-1422	0	–	–	0.04	–	1 E	110 ± 20	0.37	1.9	198	0.19
KOI-710	0	–	–	0.69	–	1 E	12.5 ± 0.7	0.12	1.7	998	0.19
KOI-623	0	–	–	0.40	–	1 E	42.2 ± 3.5	0.23	1.3	592	0.19
KOI-282	0	–	–	0.01	–	1 E	280 ± 50	0.83	1.5	**299**	0.19
KOI-620	0	–	–	0.84	–	1 E	230 ± 20	0.74	7.6	**298**	0.18
KOI-3925	0	–	–	0.38	–	1 E	17.9 ± 1.6	0.13	3.5	779	0.18
KOI-2167	0	–	–	0.05	–	1 E	260 ± 50	0.82	1.8	303	0.17
KOI-1426	0	–	–	0.02	–	1 E	290 ± 30	0.88	5.3	**294**	0.16
KOI-1127	0	–	–	0.81	–	1 E	14.2 ± 1.1	0.12	2.0	681	0.16
KOI-191	0	–	–	0.99	–	1 E	180 ± 40	0.61	3.4	301	0.16
KOI-1430	0	–	–	0.98	–	1 E	200 ± 30	0.57	3.2	**215**	0.15
KOI-806	0	–	–	0.16	–	1 E	310 ± 40	0.89	2.5	**247**	0.15
KOI-612	0	–	–	0.10	–	1 E	290 ± 40	0.79	3.6	**235**	0.15
KOI-481	0	–	–	0.02	–	1 E	160 ± 40	0.56	4.0	**282**	0.14
KOI-2714	0	–	–	0.09	–	1 E	640 ± 120	1.55	3.4	**272**	0.13
KOI-1258	0	–	–	0.96	–	1 E	430 ± 70	1.11	5.1	**218**	0.10
KOI-564	0	–	–	0.77	–	1 E	530 ± 110	1.28	4.3	**222**	0.10
KOI-1922	0	–	–	0.02	–	1 E	790 ± 220	1.69	2.9	199	0.08
KOI-2183	0	–	–	0.70	–	1 E	770 ± 190	1.64	3.0	188	0.07
KOI-518	0	–	–	0.84	–	1 E	940 ± 190	1.59	3.1	124	0.05
KOI-2842	0	–	–	0.27	–	1 E	9.5 ± 0.8	0.07	3.2	559	0.00

Notes. $^a\Delta\gamma = (\gamma_1 - \gamma_2)/\gamma_2$ where γ_1 and γ_2 are the highest and second highest γ values for that system, respectively (see BL13).

$^bR_{\max}$ is calculated by applying the lowest SNR of the detected planets in the system to the period of the inserted planet. See equation (7).

^{c}A planet number followed by 'E' indicates the planet is extrapolated (has a larger period than the outermost detected planet in the system).

$^dP_{\text{trans}}$ values ≥ 0.55 are shown in bold, indicating a higher probability to transit.

$^eT_{\text{eff}}$ values between Mars and Venus (206 to 300 K, assuming an albedo of 0.3) are shown in bold.

This paper has been typeset from a TeX/LaTeX file prepared by the author.